# Predictions of Stellar Nucleosynthetic Yields of Core Collapse Supernovae and Hypernovae on the BPASS Model*

Jingqi Sun
*The University of Auckland, New Zealand*
(Dated: 2021 Feb 19)

The recent predictions of stellar nucleosynthetic yields (SNYs) are primarily generated by the Galactic chemical evolution (GCE) model, but the binary interactions are not included effectively in the current GCE model. For the purpose of analysing the effects taken by binary stellar systems in the production of final yields for certain stellar populations, we compute the SNYs for isotopes from $^{1}_{1}$H up to $^{74}_{32}$Ge by combining the mass yields from the K06 paper [1] and both single and binary quantities from the binary population and spectral synthesis (BPASS) model [2]. The data can be matched for different masses for $10 \rightarrow 100 M_{\odot}$, and we focus on only core collapse supernovae (CCSNe) and hypernovae (HNe). We find elemental and isotopic parity (i.e. higher yields in even nuclei than odd nuclei) which can influence significantly to the final yields, this is a result of nuclear structural stability. We also confirm the dependence of yields on metallicity, increasing in yields as the growth of metallicty is often found for most elements, but specific patterns and trends vary for elements. The general patterns of BPASS yields can fit into the IMF yields for most elements, but a few violations also exist. We discover the pattern for which binary yields are basically lower than the single yields and additional HNe yields can improve the binary yields at low metallicities, appears frequently. But F is the only exception for which single yields are lower at $Z = 0.020$. We also find lower abundances for C, N and Fe in BPASS CCSNe compare to the cosmic standard, and confirm the requirement of extra sources like AGB stars. In summary, more types of stars and more accurate combining methods are required to output a more generalised result.

## I. INTRODUCTION

The stellar nucleosynthetic yields (SNYs) are used to present quantitatively the productions of possible elements and isotopes which are synthesized by nuclear fusion reactions inside the cores of stars for a certain population of stars (e.g. a galaxy or a cluster of galaxies). Along with the developments of technologies of astronomical observations in recent decades, the detailed predictions of SNYs become a crucial assignment for modern astrophysics and cosmology, as it would reveal the chemical evolutionary history in the cosmos and help human to understand the origin of elements. Current researches support that the contributions of different sources to the final yields depend on time, environment and the stellar population model used [3], hence the study for predicting the SNYs under different initial conditions and population distributions is necessary.

The types of stars which we focused on as yields sources in this project are core collapse supernovae (CCSNe) as well as their corresponding versions of hypernovae (HNe). In a nutshell, CCSNe are typical results of the deaths of massive stars ($M > 8 M_{\odot}$). More specifically, CCSNe include Type II, Type Ib and Type Ic supernovae (SNeII and SNeIb/c). Classification [4] is based on the spectral features that Type II SNe are hydrogen-rich while Type I shows no hydrogen spectrum. Moreover, Type Ib/c shows weak or no silicon absorption feature, Type Ib individually shows a further helium line while Type Ic shows weak or no helium. A hypernova is known as a very energetic supernova which referred to the extremely high energy of the explosion compared to typical CCSNe [5]. It provides an exciting possibility in advancing the binary evolution [6].

SNYs studies are basically just predictions, based on observations such like Galactic archaeology. This approach can help us to disentangle the stellar evolution of the host galaxy from the elemental abundances of the present-day stars [7]. There are recent and future observational data of elemental abundances in the Milky Way Galaxy and solar neighbourhood, combine with Galactic archaeology surveys and space astrometry missions (e.g.,Gaia), medium-resolution multi-object spectroscopy (APOGEE, HERMES, 4MOST, WEAVE, MSE) and lower-resolution multi-object spectroscopy (SDSS, RAVE, LAMOST, PFS) [7]. Together, these investigations provide evidences of theoretical predictions of the cosmic evolution of elements and isotopes. Another possible data source for the elemental proportions is the analysis of the light-curve and spectra fitting of individual SN or HN.

Based on observations and measurements of chemical enrichment sources as well as theoretical structure formations, the most current and thorough research outcomes are the Galactic chemical evolution (GCE) model (e.g. C. Kobayashi, 2020 [7]). This is the study we used as a basis for this work. The GCE model is raised from the research works of many astrophysicists for more than two decades. In general, a

*This is the Final Report for the Research Project with being supervised by Associate Professor JJ Eldridge under the course PHYSICS 309: Special Study.

relatively comprehensive predictions of almost all elemental and isotopic abundances are given by the GCE model, up to $^{238}$U (K20 [7]). Most yields sources like SNe, HNe and asymptotic giant branch (AGB) stars are included in the GCE model. However, the population of binary systems is not fully considered in the GCE model. Hence, further analysis in the binary interactions for SNYs is expected.

The Binary Population and Spectral Synthesis code (BPASS) [8] is a model of stellar populations, and it provides the core information of single and binary stellar populations in this project. BPASS model includes the binary evolution, which can take effects in the ages and spectral of an observed star, the nucleosynthetic rates and then the final yields [2]. Therefore, the binary influences are considerable in giving a significantly distinct final yields for certain elements and isotopes due to the physical properties of binary systems. For instance, if the orbits of a binary system are too closed, their gravity will cause seriously unstable reactions and even attract materials from the lighter one. In a extremer case, binaries might emerge under gravity [9]. As we know, stars are bright giant nuclear fusion reactors under a delicate equilibrium of thermal expansion and gravity, lost or gain of fuels will affect burning rates, which will then produce more certain yields for some elements or isotopes and less for some others in the ejections after explosions.

The plan of this project is as follows: We combine the nucleosynthetic yields for SNeII and HNe from the paper K06 (C. Kobayashi, 2006 [1]) with the single star and binary star populations which were computed by JJ Eldridge using the fiducial stellar models (with Hoki [10]) from the BPASS model to see the impact interacting binaries on the predicted yields from a stellar populations. We then view the results by plotting the yields for different elements and isotopes to see general patterns and outstanding features. The outline of this report is as follows: We first describe our methods of combining these datasets, key parameters, inevitable assumptions and approximations in Section 2. We present selected plots into four different subsections - all elements, specific elements, different isotopes and abundances comparisons, as our results in Section 3. We then discuss in Section 4 our findings of patterns and features for different models as well as caveats. Finally in Section 5, we summarize our conclusions.

## II. METHODS

The first pivotal data group we use in this project are the mass yields formed by SNeII and HNe of different masses from K06, with this we work out the amount of each isotope made in a Type II supernova or a hypernova for a range of stars with different effective initial masses $M_{\rm ei}$. Another core data group are the event rates for single and binary populations at different masses from the BPASS model (See Appendix A), it indicates the quantities of stars with each different $M_{\rm ei}$ for a certain population of stars. By combining the K06 SNYs with the BPASS populations, we get an approximated prediction of the SNYs made by the stellar population for both single and binary systems, thus we could see the discrepancies in their final yields and make our interpretations. Since K06 only provides yields for up to the 32th element $^{74}$Ge, we only calculated the final SNYs for up to the same isotope. Due to the short duration of this project, there are not enough resources to consider and analyse all types of stars and different models. As a result, the major objectives are CCSNe/HNe.

The first approximation has to be made in the computations is the integration method of K06 data with the populations, as K06 provides only the yields for a few mass integers, given by $M_{\rm ei} = [13, 15, 18, 20, 25, 30, 40]M_\odot$. For summing the mass integers in the populations for both BPASS and IMF, we use $8 \to 13$ for $13M_\odot$, $14 \to 16$ for $15M_\odot$, $17 \to 18$ for $18M_\odot$, $19 \to 22$ for $20M_\odot$, $23 \to 27$ for $25M_\odot$, $28 \to 34$ for $30M_\odot$ and $35 \to 100$ for $40M_\odot$. As shown, we assume that the lower limit of a supernova to be $\sim 8M_\odot$, the lower limit of a hypernova to be $\sim 18M_\odot$, and the upper limit for both SN and HN to be $\sim 100M_\odot$.

One classical stellar population distribution is the initial mass function (IMF), which gives the quantities of stars with each different $M_{\rm ei}$ for a population with a total mass $\xi_0$. This project includes the Chabrier (2003) [11] IMF for $m > 1M_\odot$, given by $\xi(m) = \xi_0 m^{-2.3}$ for both individual stars and stellar systems (e.g. binaries). We also compute the SNYs by using this IMF, as a reference group to compare against the BPASS predictions. The purpose of adding the IMF reference groups is to check the validity of BPASS on predicting SNYs, to see how BPASS differs from the commonly assumed IMF.

In modern astrophysics, metallicity $Z$ is used to describe the mass fraction of elements heavier than helium. We use $X$ and $Y$ to present the mass fractions of hydrogen and helium. For instance, the solar metalicity is $Z_\odot = 0.02 = 2\%$, which means 2% of the initial mass of the Sun are metals which are defined to be not hydrogen $X$ or helium $Y$. In the predictions of SNYs, metallicity plays a key initial parameter which will affect nuclear processes as well as final yields of each elements and their isotopes, it depends on the generation and the environment of formation (i.e. when and where the star forms) of the star. To make the GCE models data be accessible, we do not use the metallicity as a continuous function, but four significant points, as $Z = 0.00001, 0.001, 0.004, 0.020$.

Another assumption also has been made in the anal-

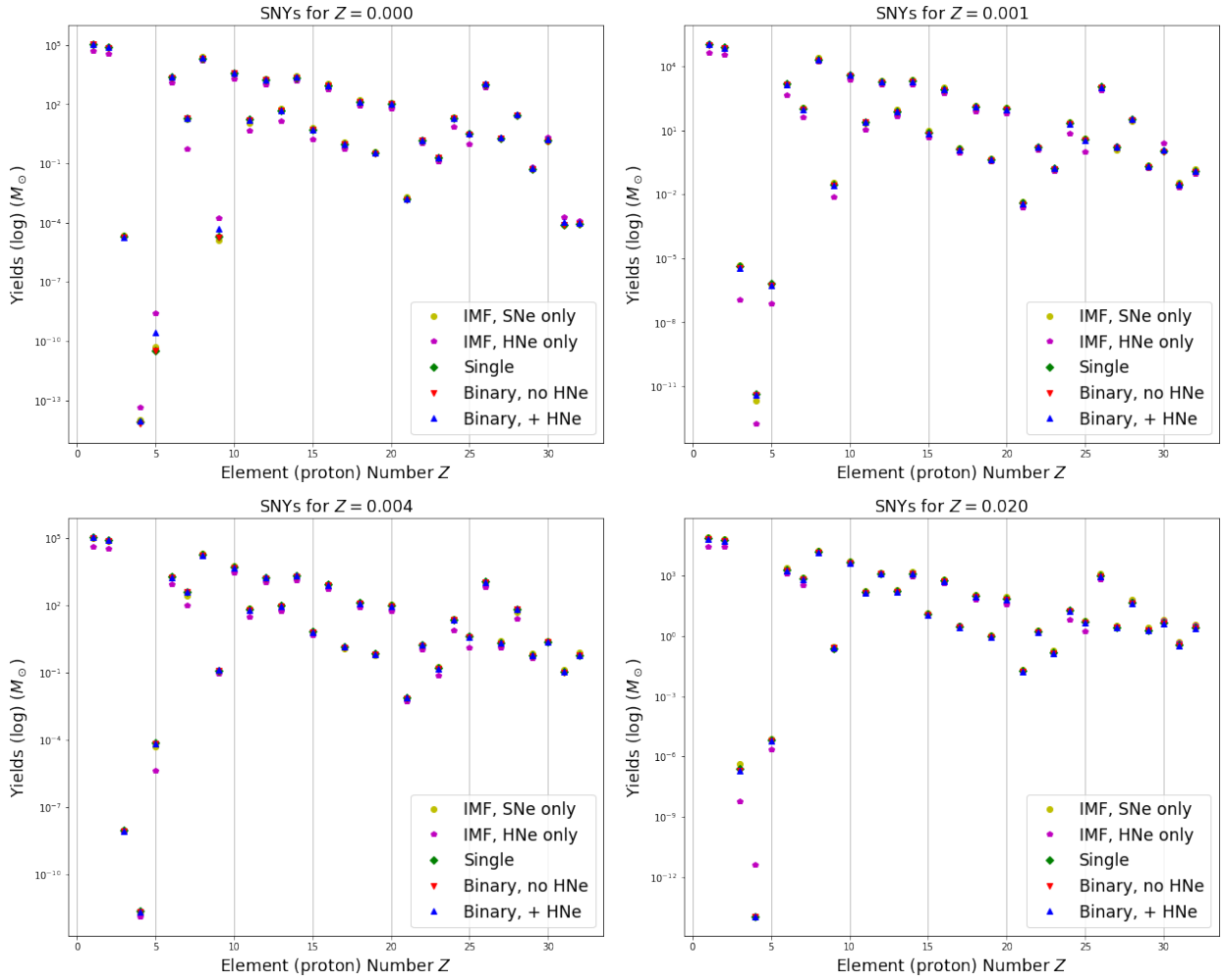


FIG. 1: The top-left plot is for $Z = 0.00001$, corresponding to the first/primordial generation of stars. At this low metallicity, BH shows a significantly high yields in boron and fluorine compare to BN. The top-right plot is for $Z = 0.001$, the bottom-left plot is for $Z = 0.004$ and the bottom-right plot is for $Z = 0.020$, which is corresponding to the solar metallicity. Due to the logarithmic scale, there are no clear numerical divergences appear between the three BPASS groups for $Z = 0.001, 0.004, 0.020$. A common pattern under all metallicties are the elemental parity (i.e. the odd-even nuclei) for elements greater than B (atomic number $> 5$), that is, the final total yields of an element with an even number of protons must be higher than its two proximate elements (which must have an odd atomic number).

ysis. We treat SNeII and SNeIb/c equivalently as they have been scaled by their metal core masses. The divergences on their outer shells will only affect significantly the yields of hydrogen and helium as well as their few isotopes. As far as we know, hydrogen and the most of helium are primarily produced during the Big Bang Nucleosynthesis (BBN) epoch, elements heavier than $\alpha$ are synthesized iteratively by stellar nuclear fusion and then ejected in SNe and HNe explorations. Thus, we focus on the metal yields than non-metal yields. Therefore, we could use the same groups of K06 yields data for both SNeII and SNeIb/c in the BPASS populations, as we assume that CCSNe with the same $M_{\rm ei}$ will produce the same amount of metal yields regardless of their SNe type (i.e. show hydrogen or not).

In the coding procedure during the research, I defined a SNYs function to give the final yields of the isotopes for the first 32 elements. The function can print yields for different metallicities, different models of populations and stellar types. The function is in the form of $Y(Z, b, h)$, where the three parameters are the initial metallicity $Z$, the distributional type of stellar populations $b$ and the novae type $h$, defined for $Z \in \{0.000, 0.001, 0.004, 0.020\}$ and $b, h \in \{0, 1, 2\}$. If $b = 0$, then the population distribution is given by the Chabrier (2003) IMF $\xi(m) = \xi_0 m^{-2.3}$ with a BPASS-scaled total mass of $\xi_0 = 2.5 \times 10^5 M_\odot$, moreover, it is BPASS single populations for $b = 1$ and is BPASS binary populations for $b = 2$. If $h = 0$, then it will output only the SNe (the sum of Type II and Ib/c) yields, if $h = 1$ it will output only the HNe yields and it will print the total yields of SNe and HNe if $h = 2$. There is another function which is used to transfer the isotope array of 83 length to an elemental array of 32 length by summing the isotopes for the same element.

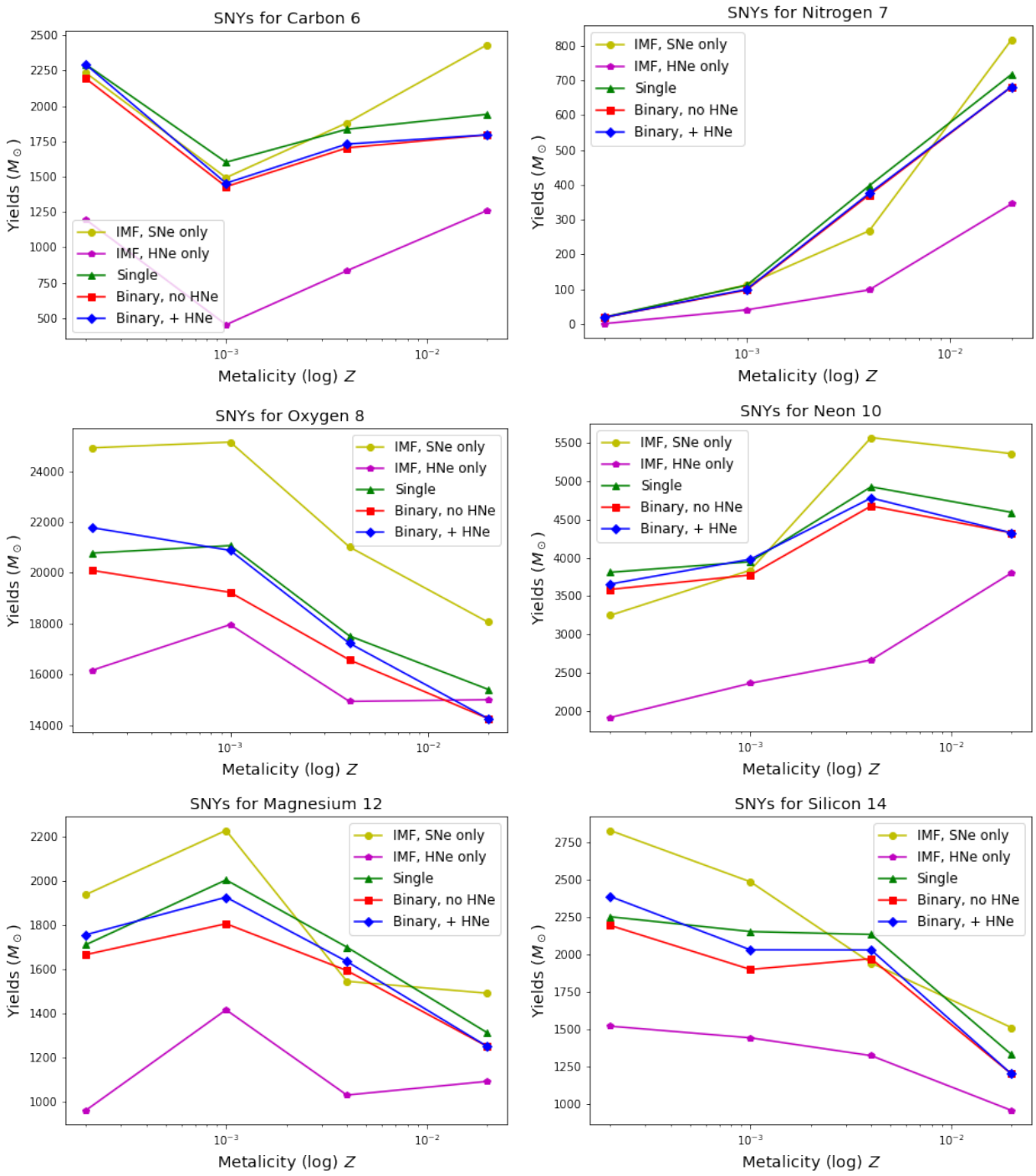


FIG. 2: The top-left plot is C, Type V with a valley at $Z = 0.001$; the top-right plot is N, Type between L1 and E1; the middle-left plot is O, Type L2; the middle-right plot is Ne, Type $\Lambda$ with a peak at $Z = 0.004$; the bottom-left plot is Mg, Type $\Lambda$ with a peak at $Z = 0.001$; the bottom-right plot is Si, Type S2. Notice that, C and Ne show strong K patterns, while O, Mg and Si show clear weak K patterns, N shows no clear K pattern, gives that HNe produce no N in the binary model. The BPASS predictions (SG, BN, BH) of O are clearly lower than the FS line for all metallicities with the the same general trend, and for both Mg and Si, the BPASS lines predict less yields than FS except for $Z = 0.004$. Another common pattern observed in these plots is the lower predictions by the BPASS model at $Z = 0.020$, about $15\% \sim 25\%$ less than the FS predictions. Generally, the BPASS lines make acceptably good approximations to the FS lines.

## III. RESULTS

On the following plots, there are five groups of population distribution shown. The two IMF groups are reference groups, used to see how much the simplest model suggests the final yields for SNe and HNe. As no HNe populations exist in the single model, there are only three BPASS groups. The five types of points/lines corresponding to five groups of SNYs, they are simplified to:

**FS:** $(b, h) = (0, 0)$, IMF, SNe only, major ref group.

**FH:** $(b, h) = (0, 1)$, IMF, HNe only, minor ref group.

**SG:** $(b, h) = (1, 0)$, BPASS, Single.

**BN:** $(b, h) = (2, 0)$, BPASS, Binary, without/no HNe.

**BH:** $(b, h) = (2, 2)$, BPASS, Binary, with/+ HNe.

### A. SNYs for All Elements

The first group of plots (FIG. 1) is the yields -vs- elemental numbers under different population, four plots for four points of metallicities. The yields are logarithmic, since the final yields for hydrogen and helium (in fact, these are the burning remnants of hydrogen and helium) are far higher than other elements. For example, the final yields of hydrogen is higher for 17 orders of magnitude than beryllium at $Z = 0.00001$. An important property has been observed - the elemental parity, which cause by odd-even nuclei.

### B. SNYs for Certain Elements

The second group of plots (FIG. 2, 3) is the yields -vs- metallicities under different population, for different elements. The yields are the sum of isotopes of a certain element and are real scaled, so we could see the detailed differences caused by different population distributions under different metallicities. We classify the tending patterns of the plots to six types:

**E.** Exponentially growth (E1) or reduce (E2), happens frequently for heavier elements.

**S.** Slowly or gently growth (S1) or reduce (S2), this kind of patterns has no strong fluctuations.

**L.** Linearly growth (L1) or reduce (L2), show a strong linear pattern, usually between the degrees of Type E and Type S.

**P.** Plain, only small fluctuations, no clear growth or reduce pattern.

**V.** Valley (V) or peak ($\Lambda$), that is, exists a unique, clear valley or peak in the yields.

**N.** None of above, no simple pattern shown.

Another common pattern in the plots, is that the SG yields are always higher than the BN yields. This might be the result of reaction rates reduction of binaries, that is, the decreasing in the nuclear fusion rates caused by the binary effects. Along with this pattern, for most of elements, the BH make more yields for lower metallicities than BN, but make no more yields for high metallicity ($Z = 0.02$). The additional yields caused by HNe decrease as the increasing of metallicity, and finally drop to zero at $Z = 0.020$, this is due to the BPASS HNe population for $Z = 0.020$ is a zero line. As a summary, in a plot, if SG is always higher than BN for a relative small fraction, and BH make more yields for $Z = 0.00001, 0.001, 0.004$ but BH = BN at $Z = 0.020$ with a general trend of reduction in the extra binary yields caused by HNe, then we call the plot to have a K pattern. More specifically, if BH $\lesssim$ SG, we call it is a strong K pattern, if BH $>$ SG (especially for $Z = 0.00001$), we call it is a weak K pattern.

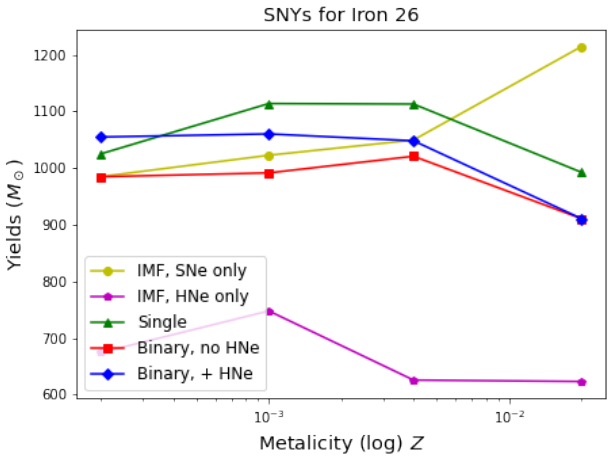


FIG. 3: Fe is Type P and shows a clear weak K pattern. Like most elements, the BPASS models predict $\sim 20\%$ less iron yields than the FS prediction at $Z = 0.020$.

In this section, we will only show the plots and detailed analysis for important elements like C, N, O, Ne, Mg, Si and Fe, for all plots please see in the Appendix B. According to the full results in Appendix B, we see that H, He, C, Ne, Al, Cr and Mn show strong K patterns, O, Mg, Si, P, S, Cl, Ar, K, Ca, Ti, V, Fe, Co, Ni and Zn show weak patterns, Li, Be, B, N, F, Na, Sc, Cu, Ga and Ge show no or unclear K patterns. As observed, almost all elements heavier or equal to Mg show weak K patterns, except Cr and Mn show clear strong K patterns and few others show unclear patterns because of extremely small divergences between lines. In the other hand, lighter elements mainly show strong K patterns, like H, He, C and Ne. One exception to the K patterns which must be mentioned is fluorine, it is the only element which binaries produce more F yields than singles at high metallicities. In summary, most elements have K patterns.

### C. SNYs for Different Isotopes

The third group of plots (FIG. 4, 5) is the yields -vs- metallicities under different population, for different isotopes of a certain element. Since the lines

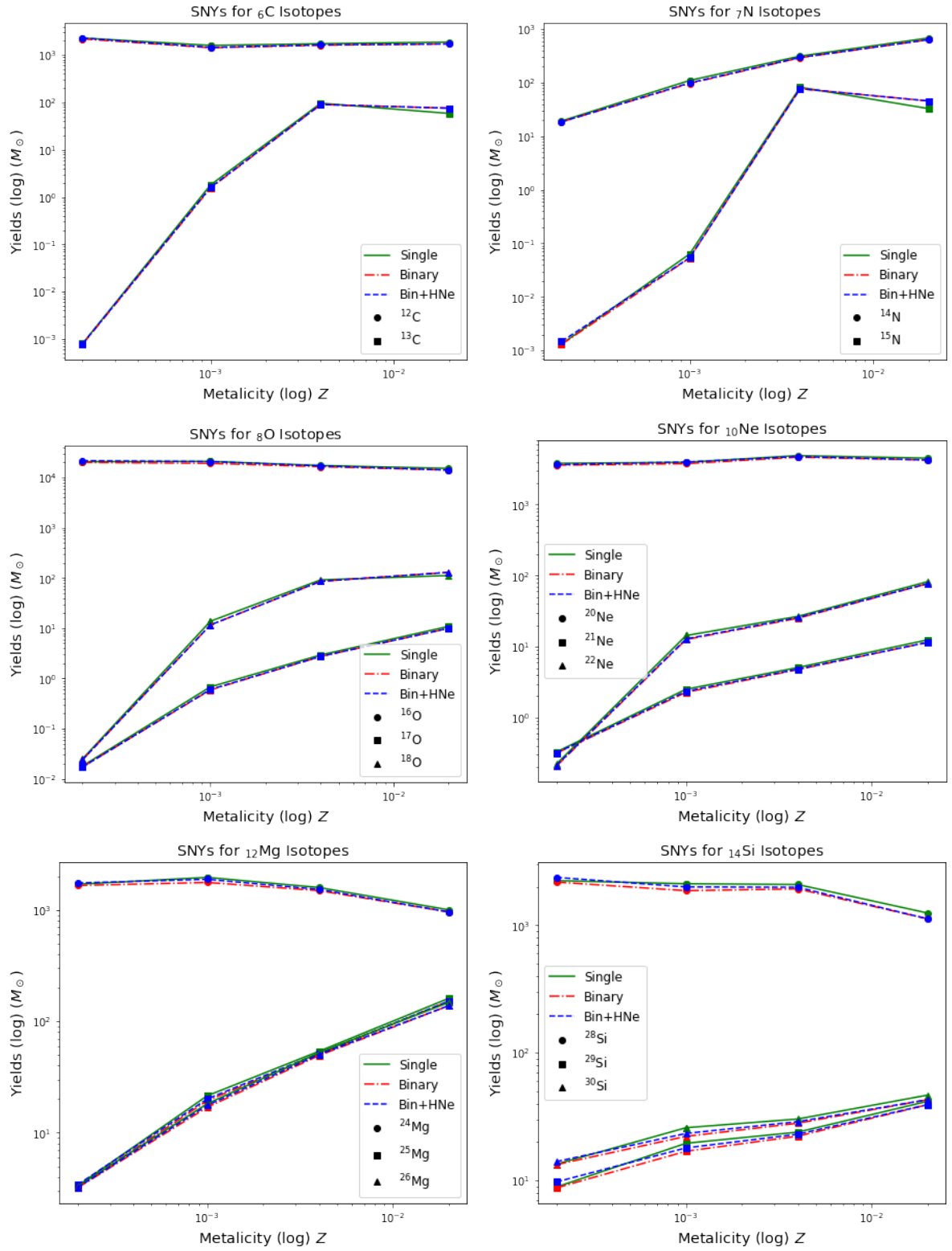


FIG. 4: First notice that, all dominant isotopes of the six elements are even and relatively stable ($^{12}$C and $^{16}$O are Type S2, $^{14}$N is Type M1, $^{20}$Ne is Type S1, $^{24}$Mg and $^{28}$Si are Type S2), and have the same numbers of protons and neutrons. The top-left C and the top-right N have similarities in their minor isotopes ($^{13}$C and $^{15}$N), both of them are Type R1 and odd, reach a small peak at $Z = 0.004$ and are predicted more yields at $Z = 0.020$. The middle-left O, the middle-right Ne, the bottom-left Mg and the bottom-right Si also have similarities in their minor isotopes, there are primarily two minor isotopes for each of them. For O and Ne, all of their minor isotopes ($^{17}$O and $^{18}$O, $^{21}$Ne and $^{22}$Ne) are Type R1 with one odd and one even, the even minors are higher than the odd minors, except for Ne at $Z = 0.00001$. All isotopes of Mg and Si show weak K patterns, and all of their minor isotopes are very closed numerically, but both $^{25}$Mg and $^{26}$Mg are Type M1 and both $^{29}$Si and $^{30}$Si are Type S1.

increase multiplied, we consider only the differences for BPASS groups (SG, BN and BH). Since the yields between isotopes can be significantly distinct, we use the logarithmic scales for both metallicity axes and yields axes.

For the same reason of simplicity, I make another group of classification for the isotope plots. First, an odd or even isotope is an isotope whose nucleon number $A$ is odd or even. As all three BPASS lines remain, I will keep using the definitions of K patterns if appropriate. Since the plots are logarithm, the exponential properties could be covered, so we use only the general changing speed as classification for each isotopes. Along with the increasing of metallicities, they are defined as:

**S.** Slowly growth (S1) or reduce (S2), this kind of patterns is usually a straight line with a tiny slope.

**R.** Rapidly growth (R1) or reduce (R2), show a relatively high slope, usually has an approximately exponential pattern.

**M.** Moderately growth (M1) or reduce (M2), usually shows a clear slope, but cannot reach the level of Type R.

**P.** Plain, no clear growth or reduce pattern.

Same as the previous section, we will only show the detailed analysis for C, N, O, Ne, Mg, Si and Fe, for all plots please see in the Appendix C.

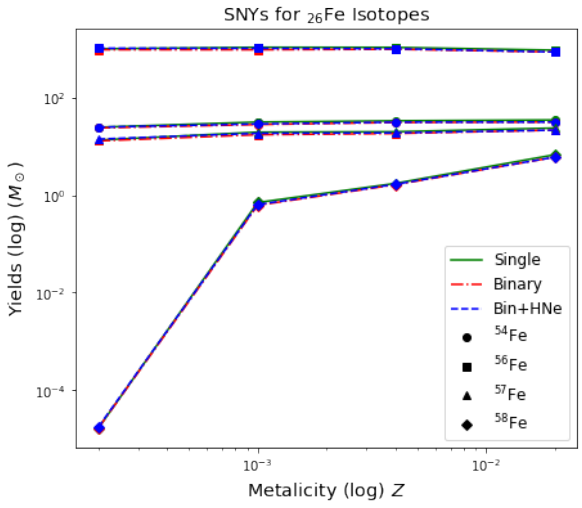


FIG. 5: All $^{54}$Fe, $^{56}$Fe and $^{57}$Fe are Type P, while $^{58}$Fe is Type R1. Notice that the dominant iron isotope is $^{56}$Fe. Iron isotopes give a general pattern for the majority of chemical metals.

### D. Abundance Comparison

In this section we will make comparison for the relative abundances of C, N, Ne, Mg, Si and Fe with the cosmic standard, to see if it need extra sources to produce those elements or not. The cosmic standard abundances data (TABLE I) we use is from (M.-F. Nieva, 2012 [12]), given by the following table. Here the second column is the relative atomic mass (RAM), in atomic mass units, the third column is the number of atoms per $10^6$ H nuclei and the fourth column is the relative ratio compare with oxygen, as cosmic standard ratios of relative abundances.

TABLE I: Cosmic Standard Abundances

| Element | RAM (u) | Atoms N. | $R_{\mathrm{X,CS}} = \mathrm{X/O}$ |
|---|---|---|---|
| C | 12.011 | $214 \pm 20$ | 27.94% |
| N | 14.007 | $62 \pm 6$ | 9.44% |
| O | 15.999 | $575 \pm 66$ | 100% |
| Ne | 20.180 | $123 \pm 14$ | 26.98% |
| Mg | 24.305 | $36.3 \pm 4.2$ | 9.59% |
| Si | 28.085 | $31.6 \pm 3.6$ | 9.65% |
| Fe | 55.845 | $33.1 \pm 2.3$ | 20.09% |

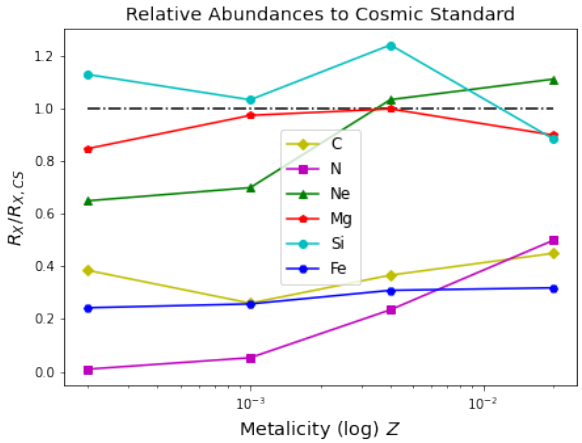


FIG. 6: C, N and Fe relative abundances are apparently lower than a half of the their cosmic standard level, while Ne, Mg and Si are relatively closed to their standard level. In the other hand, Mg, C and Fe are relatively stable as the growth of meatllicity, Mg has the least standard deviation to its cosmic average level. Si, Ne and N have much dependence on the metallicity, higher relative abundances observed for higher metallicity for Ne and N, but Si appears a more complex pattern.

We compute the BPASS SNYs for each element at each metallicity by averaging the SG yields and BH yields. Then BPASS SNYs can be used to calculate the relative abundances compare to oxygen at each metallicity, and we plot them as above (FIG. 6). The black dash-dot line is the cosmic standard abundances, independent of element and metallicity. If the $R_{\mathrm{X}}/R_{\mathrm{X,CS}}$ ratio of an element X is closed to the standard line, then it implies that the yields in CCSNe/HNe of this element approximate to its cosmic average level, hence extra sources might not be necessary to contribute to its abundances, or extra sources produce a similar level of this element as CCSNe/HNe.

And lower than the standard line can clearly indicate the requirement of extra sources to produce this element with a higher level.

As a result, C, N and Fe require additional sources to reach their cosmic standard levels, their extra sources must provide higher levels of abundances than the cosmic average to balance the total yields. While Mg yields reach the cosmic average level for a range of metallicities, and extra sources will provides a similar level to the cosmic standard. For Si and Ne, they has a strong dependence on metallicity, so the requirements of extra sources also depend on the metallicities of the sources.

## IV. DISCUSSION

For the yields comparisons between elements, a key property observed is the elemental parity caused by odd-even nuclei. The elemental parity might be the result of nuclear structural stability, that is, even nuclei have higher nuclear bonding energy per nucleon than odd nuclei, so it requires more energy and/or time to break the structure of the atom of an even element to fuse it into a heavier element. It also leads to the result more isotopes of even elements exist in the nature and are observed in the isotope section, as even elements are more stable and have the capacities to receive more neutrons to share their nuclear bonding energies.

Another significant common pattern exists in both certain elements and isotopes section is the K pattern. The physical meaning of K patterns is that the binary interactions will reduce the final yields of the element compare to the single stars scenario, confirm the theoretical prediction of which binaries will produce relatively less yields for most elements. Moreover, K patterns also imply that HNe will contribute to the final SNYs especially for the early generations of stars which are corresponding to lower metallicities. Further, strong K patterns mean that binaries can always produce less or equal SNYs no matter if HNe contributions are included, while weak K patterns agree that at some metallicities (especially at $Z = 0.00001$ for our results), with the additional yields ejected by HNe, binaries could produce more SNYs than single populations. The observation of which most elements have K patterns might be a result of the nature of binary interactions and hypernovae mechanism. In addition and in general, the BPASS predictions make acceptable approximations to most elements compare to the IMF reference group lines.

If we move forward to the full results of isotopes in Appendix C, both nucleon parity and K patterns are observed in isotope plots. For isotopes, the parity is no longer a property of the number of protons but of total nucleons. Most isotopes with an even number of total nucleons or an even number of neutrons will have more yields compare to odd isotopes, this property is outstanding especially for lighter elements for their relatively simple nuclear structures. The K patterns of isotopes are not apparently shown on the plots, but do exist as following their elemental summations. The increasing of metallicities takes a significantly effect in rare isotopes, especially for the minor isotopes which are usually heavier than the dominant isotopes. Some isotope dose not exist in the yields for low-metallicity stars, but when metallicity grows up, the yields of this isotope increase exponentially with a extremely high factor.

Compare to cosmic standard abundances, we find that extra sources are required for most elements, to balance the average yields. One possible explanation to these phenomenons is that different sources will contribute to some certain element at higher levels than the average, due to different stellar structures (e.g. mass, environment).

There are some assumptions and approximations made during computations and analysis, however, these could make unexpected large errors in the final results. For instance, as we find several peaks and valleys in the plots for certain elements versus metallicities, the model agrees with the possibility that some element may reach an extreme value (maximum or minimum) of their yields at some metallicity, but as our metallicities are points rather than a continuous function, we are not able to find where the specific metallicity is for all elements, hence the patterns shown on the plots may not fit the real situations. Furthermore, as the stellar masses we used for matching K06 yields data and BPASS populations data are also not continuous and even divided into partitions, the relative uncertainties lie in the combining and approximating procedures could be effective, hence, the final results do not have a high accuracy in the experimental sense.

CAVEATS: There are other potential chemical enrichment sources, such as AGB stars. In fact, the further stages of AGB stars, such as Type Iax supernovae (SNeIax) and electron-capture supernovae (ECSNe), should be considered as having a significant contribution towards the final yields, but we only analyse the typical CCSNe in this project. Therefore, a few differences in the average proportions of our current SNY predictions are expected for some elements.

## V. CONCLUSION

In this project, we confirm the elemental parity in both proton numbers and nucleon numbers, reveal the physics that atoms with an even number of protons or nucleons are frequently more stable than their approached odd atoms. The dependence of SNYs on

metallicities are also confirmed for most elements from H ($A = 1$) to Ge ($A = 87$), but the specific patterns and trends are not the same for each element, though they could be classified to several types. The relations between three BPASS populations can be summarised to the K pattern defined in early sections, the binary yields for high-metallicity CCSNe systems are always fewer than the single CCSNe, except for fluorine. But at low metallicties, the binary systems with including HNe can produce more yields for oxygen and more heavier elements. In general, BPASS predictions could match the IMF referenced predictions with a relatively non-ignorable average deviation. Finally, by comparing the relative abundances to oxygen in our results for C, N, Ne, Mg, Si and Fe to the cosmic standard, we confirm the requirement for additional SNYs sources to balance the elemental abundances of CCSNe/HNe for several elements, more or less.

## VI. ACKNOWLEDGEMENT

Firstly great thanks to Associate Professor JJ Eldridge, the new Head of Department of Physics, the supervisor of this project, who gave me a precious opportunity to conduct this research. Also thanks the Stars 'n' Supernovae Group, whose members gave me academic suggestions and programming supports, with kindness and enthusiasm. Finally thanks to my family, who supported me both mentally and financially as always.

[1] Chiaki Kobayashi, Hideyuki Umeda, Ken'ichi Nomoto, Nozomu Tominaga, and Takuya Ohkubo. Galactic Chemical Evolution: Carbon through Zinc. *Astrophys. J.* , 653(2):1145–1171, December 2006.

[2] J. J. Eldridge, E. R. Stanway, L. Xiao, L. A. S. McClelland, G. Taylor, M. Ng, S. M. L. Greis, and J. C. Bray. Binary population and spectral synthesis version 2.1: Construction, observational verification, and new results. *Publications of the Astronomical Society of Australia*, 34, 2017.

[3] Chiaki Kobayashi, Amanda I. Karakas, and Hideyuki Umeda. The evolution of isotope ratios in the Milky Way Galaxy. *Monthly Notices of the Royal Astronomical Society*, 414(4):3231–3250, July 2011.

[4] Massimo Turatto. Classification of supernovae. *Lecture Notes in Physics*, page 21–36, 2003.

[5] Hans-Thomas Janka. Explosion mechanisms of core-collapse supernovae. *Annual Review of Nuclear and Particle Science*, 62(1):407–451, Nov 2012.

[6] T. M. Tauris, N. Langer, T. J. Moriya, Ph. Podsiadlowski, S.-C. Yoon, and S. I. Blinnikov. Ultra-stripped type ic supernovae from close binary evolution. *The Astrophysical Journal*, 778(2):L23, Nov 2013.

[7] Chiaki Kobayashi, Amanda I. Karakas, and Maria Lugaro. The Origin of Elements from Carbon to Uranium. *Astrophys. J.* , 900(2):179, September 2020.

[8] J. Eldridge and E. R. Stanway. Bpass - binary population and spectral synthesis `https://bpass.auckland.ac.nz/`.

[9] Z. Kopal. *The Roche Problem.* Kluwer Academic, 1989.

[10] Heloise Stevance, J. Eldridge, and Elizabeth Stanway. Hoki: Making BPASS accessible through Python. *The Journal of Open Source Software*, 5(45):1987, Jan 2020.

[11] Gilles Chabrier. Galactic stellar and substellar initial mass function. *Publications of the Astronomical Society of the Pacific*, 115(809):763–795, Jul 2003.

[12] M. F. Nieva and N. Przybilla. Present-day cosmic abundances. A comprehensive study of nearby early B-type stars and implications for stellar and Galactic evolution and interstellar dust models. *Astronomy & Astrophysics*, 539:A143, March 2012.

## APPENDIX

Here I will put all sources and visual outcomes of the experimental data in this project. Appendix A is the original population data of CCSNe/HNe from the BPASS model which used for computing the final SNYs. Appendix B are the plots of all elements from H to Ge and Appendix C are the plots for all elements with more than one isotopes. For the purpose of classification and summarisation, there are detailed captions for each plot in the Appendix B and C, and there are six plots in each page.

### A. BPASS Populations

In the following tables of data, $M_{\rm ei}$ is the effective initial mass, in the unit of a solar mass $M_\odot$, and in the range of $[0, 100]M_\odot$. Notice that, the populations for Single CCHNe and Binary HNeII are zeros for all initial masses under all metallicities. Hence, here we only list the data for non-zero lines.

TABLE II: BPASS Populations for $Z = 0.000$

| $M_{\rm ei}$ | Single | | Binary | | |
|---|---|---|---|---|---|
| | SNeII | SNeIb/c | SNeII | SNeIb/c | HNeIb/c |
| $\leq$11 | 0 | 0 | 0 | 0 | 0 |
| 12 | 3203.01 | 0 | 3107.96 | 125.334 | 0 |
| 13 | 2958.99 | 0 | 2598.02 | 177.689 | 0 |
| 14 | 1707.79 | 0 | 1813.17 | 36.0245 | 0 |
| 15 | 1357.48 | 0 | 1050.86 | 10.3847 | 0 |
| 16 | 929.401 | 0 | 885.396 | 0 | 0 |
| 17 | 360.826 | 0 | 493.808 | 0 | 0 |
| 18 | 578.928 | 0 | 458.845 | 0 | 0 |
| 19 | 235.083 | 0 | 271.414 | 0 | 0 |
| 20 | 207.034 | 0 | 255.399 | 0 | 0 |
| 21 | 347.167 | 0 | 212.84 | 0 | 0 |
| 22 | 146.696 | 0 | 144.731 | 0 | 0 |
| 23 | 132.145 | 0 | 130.08 | 0 | 0 |
| 24 | 119.568 | 0 | 194.899 | 0 | 0 |
| 25 | 226.867 | 0 | 147.571 | 0 | 0 |
| 26 | 99.0258 | 0 | 20.3021 | 0 | 0 |
| 27 | 82.5051 | 0 | 16.5055 | 0 | 0 |
| 28 | 75.9744 | 0 | 108.992 | 0 | 0 |
| 29 | 70.1564 | 46.8732 | 175.592 | 2.37162 | 0 |
| 30 | 125.237 | 0 | 7.39869 | 0 | 0 |
| 31 | 56.2092 | 0 | 12.216 | 0 | 0 |
| 32 | 52.401 | 0 | 111.362 | 0 | 0 |
| 33 | 48.9503 | 0 | 82.422 | 0.000889618 | 0 |
| 34 | 88.7724 | 0 | 8.47786 | 0 | 0 |
| 35 | 41.0138 | 0 | 9.41532 | 0 | 0 |
| 36 | 38.5851 | 0 | 28.5552 | 0 | 0 |
| 37 | 36.3564 | 0 | 177.122 | 9.79358 | 11.7532 |
| 38 | 66.7247 | 0 | 8.74862 | 0 | 0 |
| 39 | 30.674 | 0 | 5.20649 | 0.0017001 | 0 |
| 40 | 29.0608 | 0 | 4.84163 | 0 | 0 |
| 41 | 27.5659 | 0 | 8.13037 | 0 | 0 |
| 42 | 26.1957 | 0 | 1.3824 | 0 | 0 |
| 43 | 24.9047 | 0 | 8.39707 | 0 | 0 |
| 44 | 23.7025 | 0 | 4.79793 | 12.7482 | 12.0149 |

Continuation of TABLE II

| $M_{\rm ei}$ | Single | | Binary | | |
|---|---|---|---|---|---|
| | SNeII | SNeIb/c | SNeII | SNeIb/c | HNeIb/c |
| 45 | 22.5814 | 0 | 82.6583 | 0 | 0 |
| 46 | 21.5343 | 0 | 57.1566 | 12.5893 | 13.5739 |
| 47 | 40.1934 | 0 | 10.2616 | 0 | 0 |
| 48 | 18.7786 | 0 | 1.66394 | 12.1136 | 12.207 |
| 49 | 17.9716 | 0 | 3.58987 | 0 | 0 |
| 50 | 17.2131 | 0 | 4.96427 | 0 | 0 |
| 51 | 16.4996 | 0 | 4.53451 | 0 | 0 |
| 52 | 15.8274 | 0 | 3.35679 | 7.82563 | 8.495 |
| 53 | 15.1936 | 0 | 5.88264 | 0 | 0 |
| 54 | 14.5953 | 0 | 48.1398 | 19.0503 | 27.3547 |
| 55 | 14.0301 | 0 | 46.2937 | 0 | 0 |
| 56 | 60.5022 | 0 | 37.1588 | 0 | 0 |
| 57 | 73.4409 | 0 | 9.38595 | 0 | 0 |
| 58 | 20.127 | 0 | 26.399 | 0 | 0 |
| 59 | 12.0557 | 0 | 9.69537 | 0 | 0 |
| 60 | 22.4451 | 0 | 3.68776 | 19.9785 | 45.8455 |
| 61 | 11.21 | 0 | 2.68233 | 0 | 0 |
| 62 | 0 | 0 | 14.1081 | 0 | 0 |
| 63 | 0 | 0 | 25.5918 | 0 | 0 |
| 64 | 10.2754 | 0 | 6.56058 | 0 | 0 |
| 65 | 18.2712 | 0 | 3.00453 | 0.502068 | 0 |
| 66 | 0 | 0 | 1.80557 | 0 | 0 |
| 67 | 0 | 0 | 1.11219 | 0 | 0 |
| 68 | 0 | 0 | 2.50412 | 0 | 0 |
| 69 | 0 | 0 | 2.07534 | 10.8484 | 36.4186 |
| 70 | 0 | 0 | 1.41894 | 0.000186201 | 0 |
| 71 | 0 | 0 | 32.1921 | 0 | 0 |
| 72 | 7.39765 | 0 | 7.94926 | 0.956192 | 0 |
| 73 | 7.18739 | 0 | 1.84323 | 0 | 0 |
| 74 | 13.7772 | 0 | 0.986066 | 0 | 0 |
| 75 | 6.6054 | 0 | 0.336086 | 0 | 0 |
| 76 | 6.42632 | 0 | 0.393392 | 6.1637 | 50.1033 |
| 77 | 4.38612 | 0 | 0 | 0 | 0 |
| 78 | 4.16995 | 0 | 1.47466 | 0 | 0 |
| 79 | 0 | 0 | 0 | 0 | 0 |
| 80 | 0 | 0 | 0 | 0 | 0 |
| 81 | 4.27609 | 0 | 0.316244 | 0 | 0 |
| 82 | 0 | 0 | 0 | 0 | 0 |
| 83 | 0 | 0 | 0 | 0 | 0 |
| 84 | 0 | 0 | 0.288133 | 0 | 0 |
| 85 | 0 | 0 | 2.17611 | 0 | 0 |
| 86 | 0 | 0 | 1.79781 | 0 | 0 |
| 87 | 0 | 0 | 0 | 0 | 0 |
| 88 | 0 | 0 | 10.3003 | 0 | 0 |
| 89 | 0 | 0 | 22.9427 | 0 | 0 |
| 90 | 0 | 0 | 3.80031 | 0 | 0 |
| 91 | 3.78094 | 0 | 1.71258 | 0 | 0 |
| 92 | 0 | 0 | 0.394225 | 0 | 0 |
| 93 | 0 | 0 | 0 | 4.08899 | 48.4787 |
| 94 | 0 | 0 | 3.52857 | 0 | 0 |
| 95 | 0 | 0 | 0.124867 | 0 | 0 |
| 96 | 0 | 0 | 1.97221 | 0 | 0 |
| 97 | 0 | 0 | 0.51934 | 0 | 0 |
| 98 | 0 | 0 | 0 | 0 | 0 |
| 99 | 0 | 0 | 0 | 0.313918 | 0 |
| 100 | 0 | 0 | 0.377746 | 0 | 0 |

TABLE III: BPASS Populations for $Z = 0.001$

| $M_{\rm ei}$ | Single | | Binary | | |
|---|---|---|---|---|---|
| | SNeII | SNeIb/c | SNeII | SNeIb/c | HNeIb/c |
| ≤11 | 0 | 0 | 0 | 0 | 0 |
| 12 | 3465.26 | 0 | 2215.54 | 291.762 | 0 |
| 13 | 3138.66 | 0 | 2805.51 | 151.639 | 0 |
| 14 | 1965.85 | 0 | 2018.24 | 1.52014 | 0 |
| 15 | 1357.48 | 0 | 988.026 | 0 | 0 |
| 16 | 505.063 | 0 | 519.901 | 0 | 0 |
| 17 | 424.338 | 0 | 635.112 | 0 | 0 |
| 18 | 670.875 | 0 | 471.995 | 0 | 0 |
| 19 | 268.879 | 0 | 279.308 | 0 | 0 |
| 20 | 235.083 | 0 | 285.75 | 0 | 0 |
| 21 | 390.558 | 0 | 289.104 | 0 | 0 |
| 22 | 163.643 | 0 | 170.632 | 0 | 0 |
| 23 | 146.696 | 0 | 153.296 | 0 | 0 |
| 24 | 132.145 | 0 | 151.991 | 0 | 0 |
| 25 | 119.568 | 0 | 233.147 | 0 | 0 |
| 26 | 226.867 | 0 | 34.988 | 0.000862274 | 0 |
| 27 | 99.0258 | 0 | 32.6603 | 1.43755 | 0 |
| 28 | 82.5051 | 0 | 28.4971 | 4.03011 | 0 |
| 29 | 75.9744 | 0 | 147.515 | 6.54872 | 0 |
| 30 | 70.1564 | 0 | 112.632 | 16.0513 | 12.9242 |
| 31 | 125.237 | 0 | 24.4089 | 17.3852 | 7.39734 |
| 32 | 56.2092 | 0 | 16.9425 | 31.0573 | 53.3061 |
| 33 | 52.401 | 0 | 107.118 | 27.7292 | 64.2859 |
| 34 | 48.9503 | 0 | 64.595 | 21.6176 | 35.8928 |
| 35 | 45.8147 | 0 | 9.99897 | 0 | 0 |
| 36 | 42.9577 | 0 | 15.7931 | 2.8167 | 0 |
| 37 | 79.5989 | 0 | 35.1805 | 3.09955 | 0 |
| 38 | 36.3564 | 0 | 157.456 | 2.09717 | 0 |
| 39 | 34.3067 | 0 | 5.37287 | 1.09641 | 0 |
| 40 | 32.418 | 0 | 11.4375 | 0 | 0 |
| 41 | 30.674 | 0 | 4.71829 | 0 | 0 |
| 42 | 29.0608 | 0 | 6.61006 | 0.000580253 | 0 |
| 43 | 27.5659 | 0 | 5.37399 | 0 | 0 |
| 44 | 26.1957 | 0 | 1.53639 | 1.01688 | 0 |
| 45 | 24.9047 | 0 | 7.95088 | 2.00976 | 0 |
| 46 | 23.7025 | 0 | 23.1232 | 4.11777 | 33.2178 |
| 47 | 22.5814 | 0 | 56.5849 | 2.55815 | 0 |
| 48 | 21.5343 | 0 | 13.8769 | 0.94405 | 0 |
| 49 | 0 | 0 | 49.9164 | 2.49132 | 0 |
| 50 | 20.5552 | 0 | 1.30534 | 2.64653 | 29.6404 |
| 51 | 19.6383 | 0 | 3.21951 | 0 | 0 |
| 52 | 18.7786 | 0 | 3.91772 | 1.03441 | 0 |
| 53 | 17.9716 | 0 | 4.92344 | 0.735907 | 0 |
| 54 | 17.2131 | 0 | 2.22303 | 3.77114 | 21.0019 |
| 55 | 16.4996 | 0 | 14.2736 | 4.42709 | 0 |
| 56 | 15.8274 | 0 | 29.6401 | 2.25617 | 9.40904 |
| 57 | 15.1936 | 0 | 4.08158 | 1.0646 | 0 |
| 58 | 14.5953 | 0 | 12.9281 | 3.87787 | 17.2865 |
| 59 | 27.5257 | 0 | 32.7551 | 1.38383 | 0 |
| 60 | 0 | 0 | 1.99974 | 0 | 0 |
| 61 | 12.9896 | 0 | 8.18966 | 1.72456 | 12.6324 |
| 62 | 12.5102 | 0 | 8.43031 | 1.1141 | 0 |
| 63 | 12.0557 | 0 | 2.11716 | 1.85541 | 0 |
| 64 | 11.6244 | 0 | 0.0778658 | 2.78936 | 0 |
| 65 | 11.21 | 0 | 11.8617 | 6.44974 | 0 |
| 66 | 21.2712 | 0 | 21.2321 | 2.57108 | 0 |
| 67 | 10.098 | 0 | 1.25971 | 2.0654 | 0 |
| 68 | 9.76229 | 0 | 27.825 | 1.4514 | 0 |
| 69 | 9.44224 | 0 | 0.541391 | 2.28765 | 0 |

Continuation of TABLE III

| $M_{\rm ei}$ | Single | | Binary | | |
|---|---|---|---|---|---|
| | SNeII | SNeIb/c | SNeII | SNeIb/c | HNeIb/c |
| 70 | 9.13694 | 0 | 4.02155 | 0.959928 | 0 |
| 71 | 8.84552 | 0 | 0 | 1.7705 | 0 |
| 72 | 8.56717 | 0 | 2.46417 | 1.42821 | 0 |
| 73 | 8.30115 | 0 | 3.94095 | 6.12043 | 0.258312 |
| 74 | 8.59254 | 0 | 1.4262 | 3.70315 | 0 |
| 75 | 8.3326 | 0 | 4.38121 | 5.77143 | 0 |
| 76 | 8.08372 | 0 | 5.26455 | 3.80156 | 0 |
| 77 | 15.243 | 0 | 11.5611 | 4.56298 | 0 |
| 78 | 7.61679 | 0 | 25.0531 | 6.88552 | 0 |
| 79 | 0 | 0 | 0.675952 | 0.795987 | 0 |
| 80 | 0 | 0 | 0 | 0.365084 | 0 |
| 81 | 0 | 0 | 0 | 0 | 0 |
| 82 | 0 | 7.18739 | 0 | 2.39035 | 0 |
| 83 | 0 | 6.98554 | 0 | 3.20619 | 0 |
| 84 | 0 | 13.3971 | 0 | 0.711063 | 0 |
| 85 | 0 | 6.42632 | 0 | 1.80565 | 0 |
| 86 | 0 | 12.3424 | 0 | 0.0163562 | 0 |
| 87 | 0 | 5.9288 | 0 | 5.20419 | 0 |
| 88 | 0 | 5.77516 | 0 | 3.12736 | 0 |
| 89 | 0 | 8.88634 | 0 | 1.93602 | 0 |
| 90 | 0 | 4.27609 | 0 | 4.23804 | 0 |
| 91 | 0 | 8.23748 | 0 | 4.85057 | 0 |
| 92 | 0 | 3.96866 | 0 | 5.04282 | 0 |
| 93 | 0 | 7.65413 | 0 | 8.62803 | 0 |
| 94 | 0 | 3.69181 | 6.27E-05 | 31.9029 | 0 |
| 95 | 0 | 46.8732 | 3.07664 | 6.17254 | 0 |
| 96 | 0 | 0 | 0 | 1.54139 | 0 |
| 97 | 0 | 0 | 0 | 0.702657 | 0 |
| 98 | 0 | 0 | 0 | 0.353677 | 0 |
| 99 | 0 | 0 | 0 | 1.09519 | 0 |
| 100 | 0 | 0 | 0 | 0.907054 | 0 |

TABLE IV: BPASS Populations for $Z = 0.004$

| $M_{\rm ei}$ | Single | | Binary | | |
|---|---|---|---|---|---|
| | SNeII | SNeIb/c | SNeII | SNeIb/c | HNeIb/c |
| ≤13 | 0 | 0 | 0 | 0 | 0 |
| 14 | 5191.16 | 0 | 3828.46 | 671.008 | 0 |
| 15 | 2074.62 | 0 | 1875.67 | 19.9701 | 0 |
| 16 | 1351.9 | 0 | 1389.81 | 0.23589 | 0 |
| 17 | 1114.65 | 0 | 936.716 | 0.892707 | 0 |
| 18 | 424.338 | 0 | 504.592 | 4.76199 | 0 |
| 19 | 670.875 | 0 | 517.746 | 6.41613 | 0 |
| 20 | 268.879 | 0 | 255.876 | 6.28826 | 0 |
| 21 | 235.083 | 0 | 233.027 | 11.917 | 0 |
| 22 | 390.558 | 0 | 255.677 | 17.8316 | 0 |
| 23 | 163.643 | 0 | 156.748 | 24.5607 | 0 |
| 24 | 146.696 | 0 | 140.725 | 17.4762 | 0 |
| 25 | 132.145 | 0 | 147.257 | 9.63153 | 0 |
| 26 | 238.226 | 0 | 176.92 | 76.4976 | 28.6914 |
| 27 | 108.21 | 0 | 78.5011 | 55.5131 | 17.4842 |
| 28 | 99.0258 | 0 | 61.311 | 64.5241 | 37.5198 |
| 29 | 82.5051 | 0 | 46.1096 | 18.3069 | 23.2775 |
| 30 | 146.131 | 0 | 145.184 | 35.8387 | 15.5453 |
| 31 | 64.9535 | 0 | 21.0844 | 14.2463 | 32.2895 |
| 32 | 165.443 | 0 | 54.8716 | 13.0822 | 16.9069 |
| 33 | 52.401 | 0 | 19.4267 | 32.0869 | 0.985921 |
| 34 | 0 | 26.1957 | 48.0207 | 18.3776 | 0.392582 |
| 35 | 0 | 0 | 7.4428 | 25.1886 | 0 |

Continuation of TABLE IV

| $M_{\rm ei}$ | Single | | Binary | | |
|---|---|---|---|---|---|
| | SNeII | SNeIb/c | SNeII | SNeIb/c | HNeIb/c |
| 36 | 0 | 0 | 7.18244 | 15.0753 | 0 |
| 37 | 42.9577 | 0 | 10.0403 | 12.8313 | 0 |
| 38 | 86.8285 | 0 | 5.68644 | 13.4963 | 0 |
| 39 | 0 | 0 | 1.20984 | 67.0987 | 0 |
| 40 | 36.3564 | 38.5851 | 6.78784 | 89.5949 | 0 |
| 41 | 0 | 66.7247 | 0 | 16.5839 | 0 |
| 42 | 30.674 | 0 | 0.792527 | 11.4758 | 0 |
| 43 | 29.0608 | 0 | 0.750847 | 6.0176 | 0 |
| 44 | 27.5659 | 48.6072 | 1.154 | 10.6859 | 0 |
| 45 | 0 | 0 | 0.996939 | 4.53042 | 0 |
| 46 | 0 | 0 | 0 | 11.0022 | 0 |
| 47 | 0 | 21.5343 | 0 | 43.3968 | 0 |
| 48 | 0 | 43.1365 | 0 | 50.7017 | 0 |
| 49 | 0 | 19.6383 | 0 | 46.6442 | 0 |
| 50 | 0 | 18.7786 | 0 | 12.4867 | 0 |
| 51 | 0 | 17.9716 | 0 | 6.85802 | 0 |
| 52 | 0 | 33.7127 | 0 | 8.98901 | 0 |
| 53 | 0 | 15.8274 | 0 | 10.7782 | 0 |
| 54 | 0 | 43.819 | 0.403062 | 25.878 | 0 |
| 55 | 0 | 0 | 0 | 55.4444 | 0 |
| 56 | 0 | 43.5721 | 0 | 6.99995 | 0 |
| 57 | 0 | 12.0557 | 0 | 10.319 | 0 |
| 58 | 0 | 22.8343 | 0 | 8.77189 | 0 |
| 59 | 0 | 21.2712 | 0 | 18.0427 | 0 |
| 60 | 0 | 29.3026 | 0 | 45.8966 | 0 |
| 61 | 0 | 26.5496 | 0 | 10.8797 | 0 |
| 62 | 0 | 16.8937 | 0 | 7.22069 | 0 |
| 63 | 0 | 24.2616 | 0 | 16.8068 | 0 |
| 64 | 0 | 15.0144 | 0 | 44.336 | 0 |
| 65 | 0 | 14.1729 | 0 | 1.23726 | 0 |
| 66 | 0 | 13.3971 | 0 | 4.39849 | 0 |
| 67 | 0 | 12.6804 | 0 | 1.46392 | 0 |
| 68 | 0 | 12.0171 | 0 | 1.32362 | 0 |
| 69 | 0 | 10.2754 | 0 | 6.84095 | 0 |
| 70 | 0 | 8.6622 | 0.3192 | 1.86995 | 0 |
| 71 | 0 | 8.23748 | 0 | 8.90483 | 0 |
| 72 | 0 | 7.84184 | 0 | 11.2565 | 0 |
| 73 | 0 | 7.47275 | 0 | 7.85222 | 0 |
| 74 | 0 | 46.8732 | 0 | 40.24 | 0 |
| 75 | 0 | 0 | 0 | 1.20905 | 0 |
| 76 | 0 | 0 | 0 | 2.68777 | 0 |
| 77 | 0 | 0 | 0 | 0.540207 | 0 |
| 78 | 0 | 0 | 0 | 2.93354 | 0 |
| 79 | 0 | 0 | 0 | 3.98401 | 10.701 |
| 80 | 0 | 0 | 0 | 1.38309 | 0 |
| 81 | 0 | 0 | 0 | 3.02944 | 0 |
| 82 | 0 | 0 | 0 | 4.89115 | 0 |
| 83 | 0 | 0 | 0 | 1.61716 | 0 |
| 84 | 0 | 0 | 0.310062 | 9.02155 | 0 |
| 85 | 0 | 0 | 0 | 8.89231 | 0 |
| 86 | 0 | 0 | 0 | 6.57311 | 0 |
| 87 | 0 | 0 | 0 | 20.6707 | 0 |
| 88 | 0 | 0 | 0 | 1.23647 | 0 |
| 89 | 0 | 0 | 0 | 1.50752 | 0 |
| 90 | 0 | 0 | 0 | 2.85795 | 0 |
| 91 | 0 | 0 | 0 | 1.29705 | 0 |
| 92 | 0 | 0 | 0 | 1.89996 | 0 |
| 93 | 0 | 0 | 0 | 1.04262 | 0 |
| 94 | 0 | 0 | 0 | 1.57502 | 0 |
| 95 | 0 | 0 | 0 | 0.777967 | 0 |

Continuation of TABLE IV

| $M_{\rm ei}$ | Single | | Binary | | |
|---|---|---|---|---|---|
| | SNeII | SNeIb/c | SNeII | SNeIb/c | HNeIb/c |
| 96 | 0 | 0 | 0 | 0.689529 | 0 |
| 97 | 0 | 0 | 0 | 0.0199628 | 0 |
| 98 | 0 | 0 | 0 | 3.23424 | 0 |
| 99 | 0 | 0 | 0 | 0.858173 | 0 |
| 100 | 0 | 0 | 0 | 3.91697 | 0 |

TABLE V: BPASS Populations for $Z = 0.020$

| $M_{\rm ei}$ | Single | | Binary | | |
|---|---|---|---|---|---|
| | SNeII | SNeIb/c | SNeII | SNeIb/c | HNeIb/c |
| $\leq$10 | 0 | 0 | 0 | 0 | 0 |
| 11 | 0 | 0 | 9.64092 | 13.7052 | 0 |
| 12 | 2986.23 | 0 | 1753.73 | 519.593 | 0 |
| 13 | 1472.13 | 0 | 947.711 | 288.168 | 0 |
| 14 | 747.893 | 0 | 569.933 | 203.807 | 0 |
| 15 | 609.588 | 0 | 408.732 | 248.151 | 0 |
| 16 | 505.063 | 0 | 281.711 | 174.917 | 0 |
| 17 | 424.338 | 0 | 246.969 | 165.639 | 0 |
| 18 | 360.826 | 0 | 234.747 | 136.915 | 0 |
| 19 | 310.049 | 0 | 155.038 | 119.839 | 0 |
| 20 | 0 | 0 | 36.5814 | 136.82 | 0 |
| 21 | 268.879 | 0 | 107.778 | 122.82 | 0 |
| 22 | 235.083 | 0 | 135.694 | 133.122 | 0 |
| 23 | 0 | 0 | 55.7605 | 174.05 | 0 |
| 24 | 207.034 | 0 | 48.1172 | 74.5258 | 0 |
| 25 | 183.524 | 0 | 110.267 | 20.9738 | 0 |
| 26 | 163.643 | 0 | 92.212 | 146.003 | 0 |
| 27 | 146.696 | 0 | 62.1779 | 192.846 | 0 |
| 28 | 132.145 | 0 | 58.5877 | 130.381 | 0 |
| 29 | 119.568 | 75.9744 | 79.1626 | 90.4317 | 0 |
| 30 | 118.657 | 0 | 119.035 | 151.512 | 0 |
| 31 | 207.235 | 15.8069 | 18.9444 | 35.0464 | 0 |
| 32 | 0 | 35.3213 | 18.5847 | 7.28093 | 0 |
| 33 | 0 | 216.543 | 0.99089 | 54.2333 | 0 |
| 34 | 0 | 396.254 | 0 | 233.557 | 0 |
| 35 | 0 | 449.937 | 0 | 293.016 | 0 |
| 36 | 0 | 67.5117 | 0 | 26.2232 | 0 |
| 37 | 0 | 43.819 | 0.641208 | 142.792 | 0 |
| 38 | 0 | 59.2886 | 0 | 102.992 | 0 |
| 39 | 0 | 63.0431 | 0 | 34.3691 | 0 |
| 40 | 0 | 196.34 | 0 | 200.091 | 0 |
| 41 | 0 | 30.1377 | 0 | 6.33045 | 0 |
| 42 | 0 | 0 | 0 | 3.48439 | 0 |
| 43 | 0 | 0 | 0 | 1.06541 | 0 |
| $\geq$44 | 0 | 0 | 0 | 0 | 0 |

### B. All Plots for Elements

The plots start on the next page.

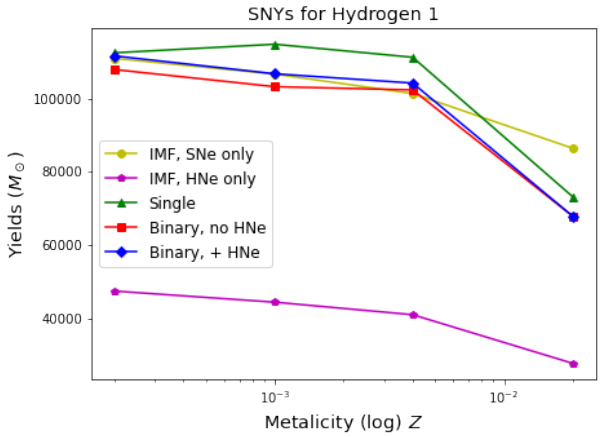


FIG. 7: H, Type S2, shows a strong K pattern. The BPASS lines make good approximations to the FS line, but the BPASS predictions agree with less amount of hydrogen remnant at $Z = 0.020$.

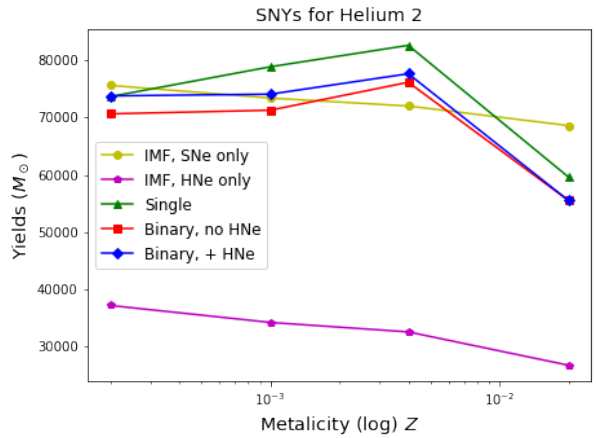


FIG. 8: He, Type $\Lambda$ with a relative small peak at $Z = 0.004$, shows a strong K pattern. The BPASS lines make not so good approximations to the FS line, the detailed patterns do not match.

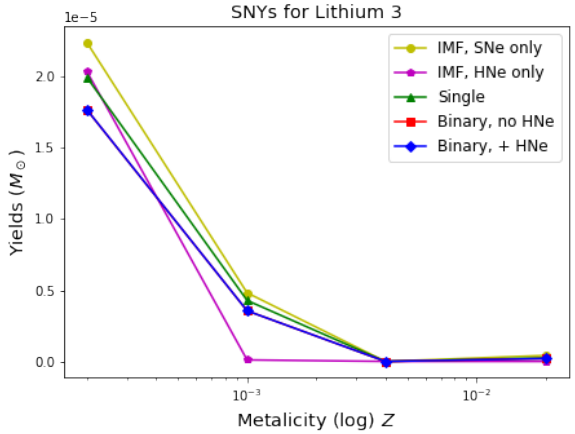


FIG. 9: Li, Type E2, shows no K pattern. BH $\sim$ BN for all metallicities, which means that HNe do not produce more lithium in the binary model. The BPASS lines make good approximations to the FS line with an acceptably lower prediction.

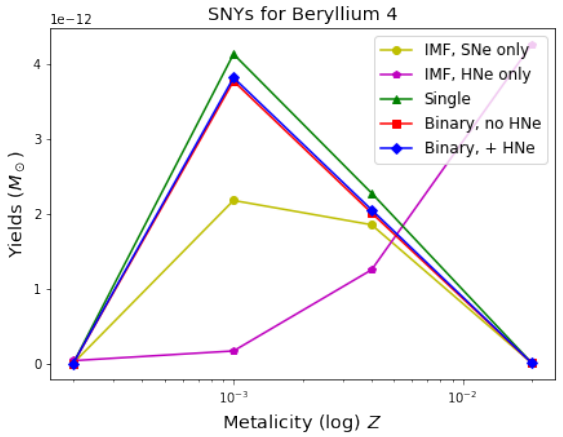


FIG. 10: Be, Type $\Lambda$ with a clear peak at $Z = 0.001$, shows no clear K pattern. The BPASS model lines predict a peak yields about twice to the FS line, and the FH line shows a distinct pattern (E1).

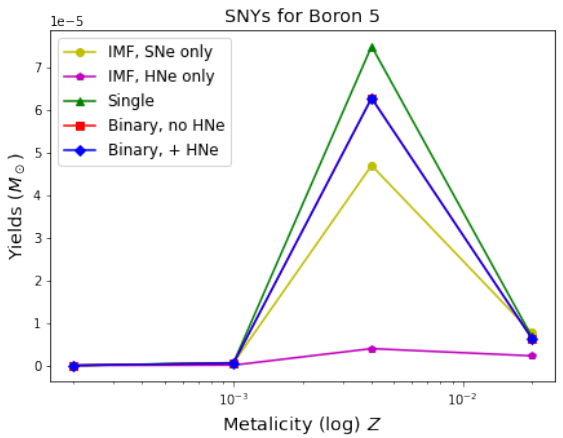


FIG. 11: B, Type $\Lambda$ with a significantly large peak at $Z = 0.004$, shows no K pattern. BH $\sim$ BN for all metallicities implies that HNe produce no boron in the binary model. Similar to Be, the BPASS lines predict a peak yields about twice to the FS line with the same pattern.

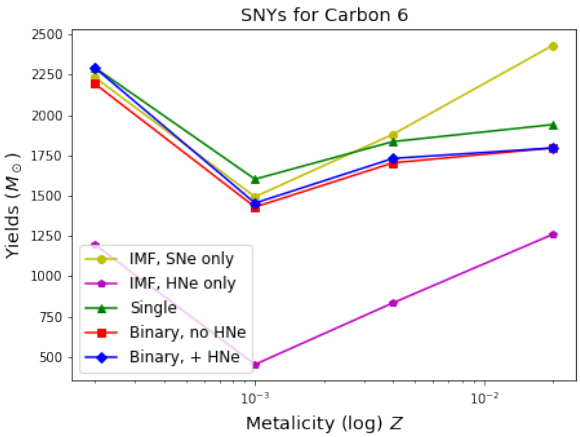


FIG. 12: C, Type V with a relative small valley at $Z = 0.001$, shows a strong K pattern. The BPASS lines make good approximations to the FS line, but the BPASS model predicts $\sim 30\%$ less carbon yields at $Z = 0.020$.

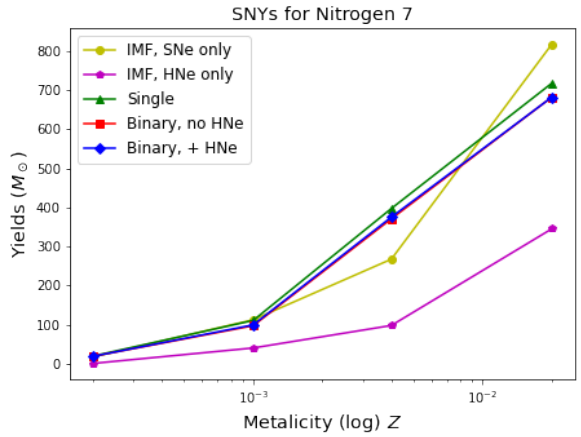


FIG. 13: N, Type L1, shows no clear K pattern. The BPASS lines make good approximations to the FS line, BH ∼ BN for all metallicities gives that HNe produce no nitrogen in the binary model.

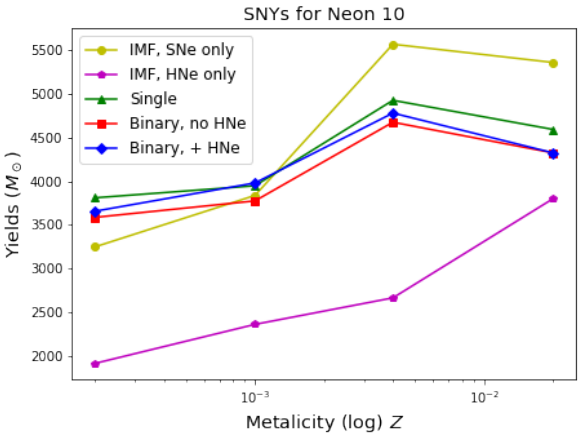


FIG. 16: Ne, Type Λ with a small peak at $Z = 0.004$, shows a strong K pattern. The BPASS predictions give less neon yields for $Z = 0.004$ and $Z = 0.020$.

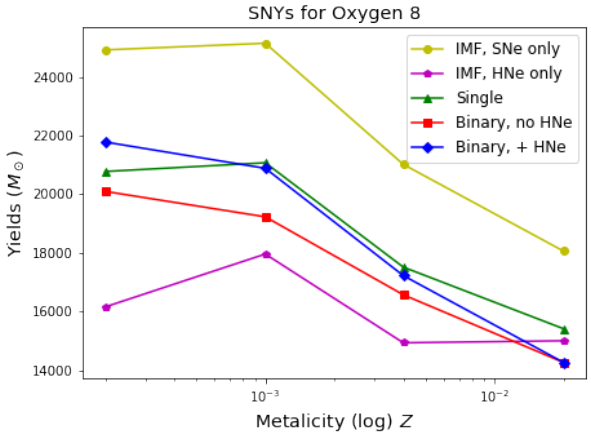


FIG. 14: O, Type L2, shows a clear weak K pattern. The BPASS predictions are clearly lower than the FS line, but the trends are the same.

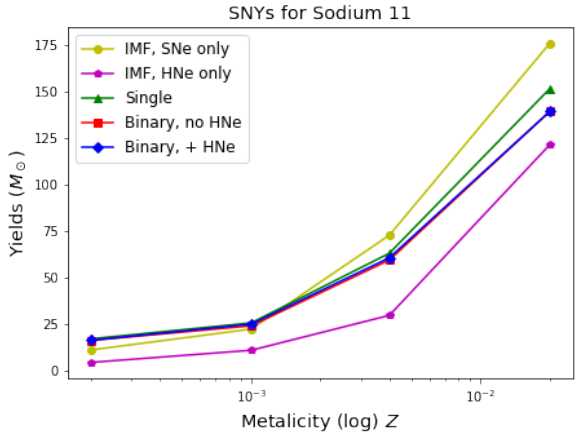


FIG. 17: Na, Type E1, shows no clear K pattern. The BPASS lines make good approximations to the FS line.

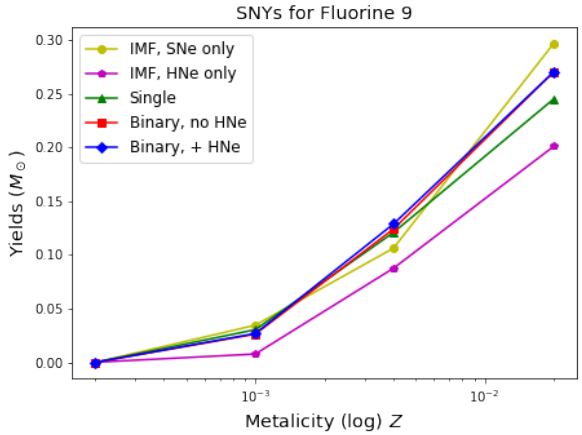


FIG. 15: F, Type E1, shows no K pattern. Fluorine is the only one in the first 32 elements which SG line predicts less yields than BN at $Z = 0.020$. The BPASS lines still make good approximations to the FS line.

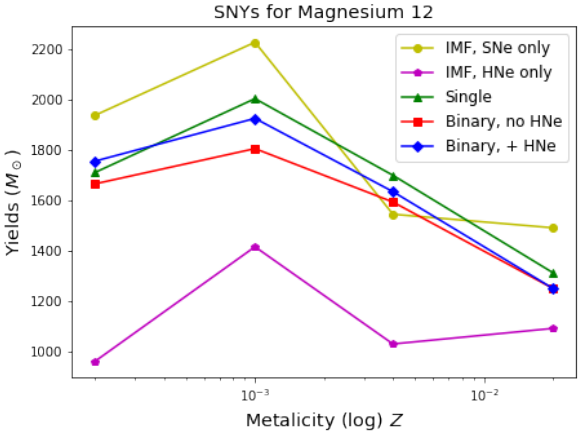


FIG. 18: Mg, Type Λ with a small peak at $Z = 0.001$, shows a weak K pattern. The BPASS predictions give less magnesium yields than FS except for $Z = 0.004$.

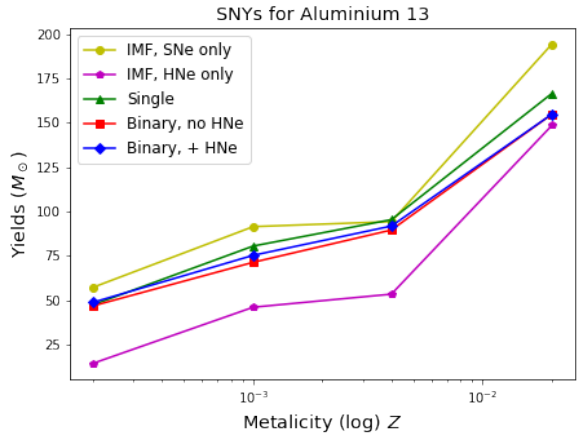


FIG. 19: Al, Type L1, shows a strong K pattern. The BPASS lines make good approximations to the FS line.

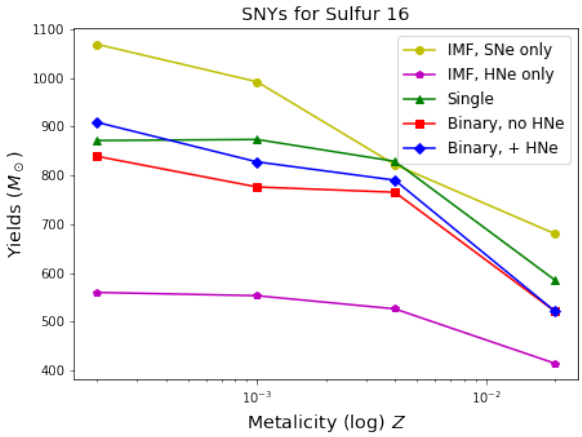


FIG. 22: S, Type S2, shows a clear weak K pattern. The sulfur yields appear a highly similar pattern as Si.

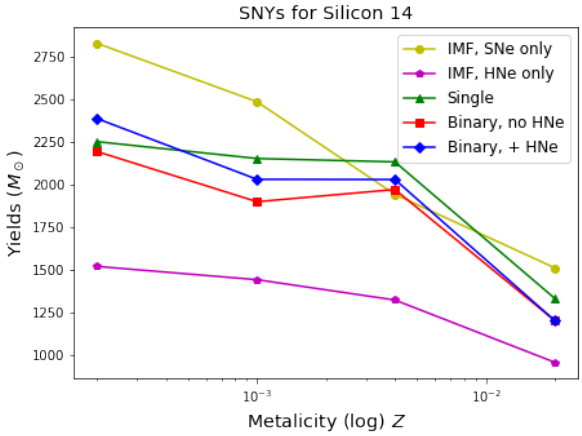


FIG. 20: Si, Type S2, shows a clear weak K pattern. Similar to Mg, the BPASS lines predict less silicon yields than FS except for $Z = 0.004$.

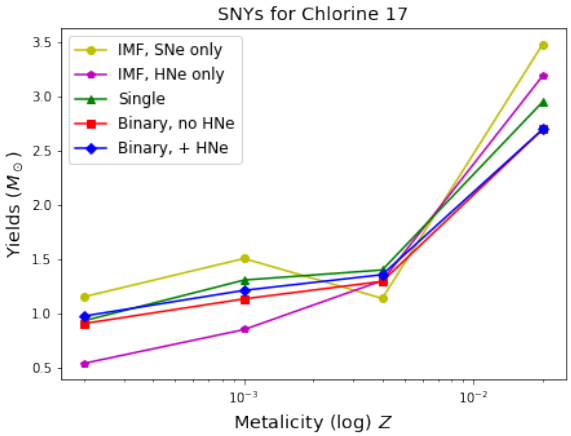


FIG. 23: Cl, Type E1, shows a weak K pattern. Its general pattern appears a relative mild version of P, especially FS.

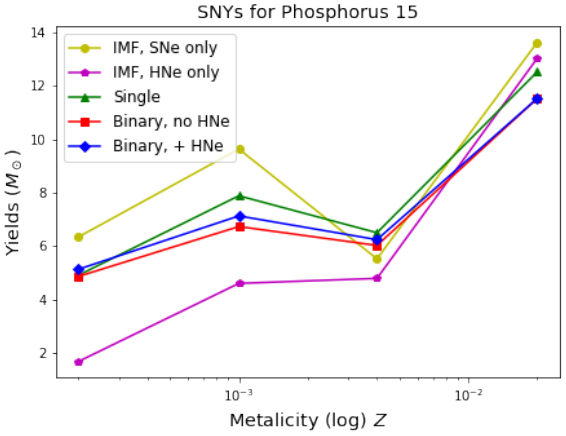


FIG. 21: P, Type N, shows a weak K pattern. The yields have a small peak at $Z = 0.001$ but subsequently have another valley at $Z = 0.004$, then reach their maximum at $Z = 0.020$. The BPASS lines match the general pattern of FS.

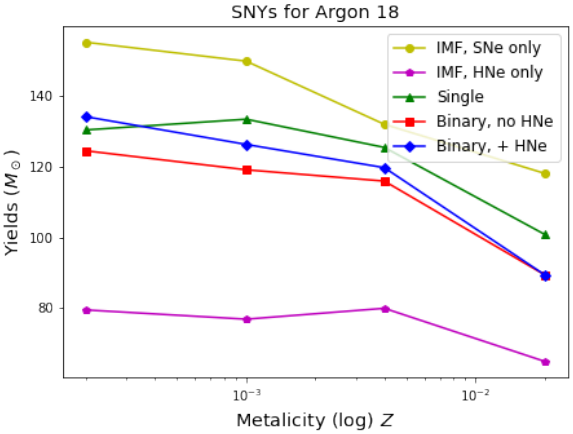


FIG. 24: Ar, Type S2, shows a weak K pattern. The BPASS lines predict less yields than FS for all metallicities with a similar general pattern.

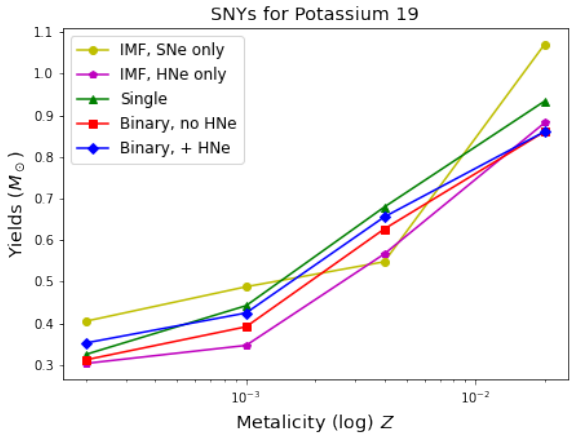


FIG. 25: K, Type L1, shows a weak K pattern. The BPASS lines make acceptable approximations to the FS line.

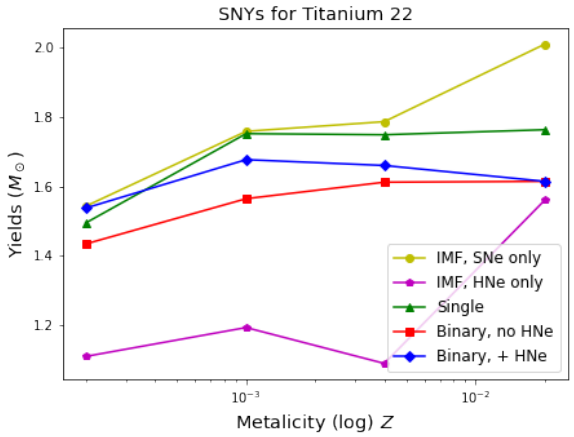


FIG. 28: Ti, Type P, shows a clear weak K pattern. The BPASS lines predict less or equal yields than FS for all metallicities, especially for $Z = 0.020$.

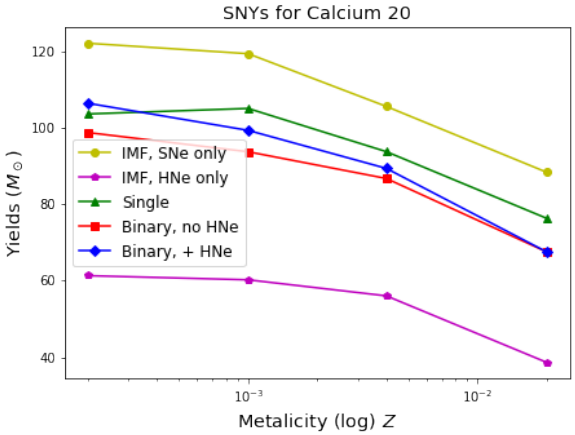


FIG. 26: Ca, Type S2, shows a weak K pattern. Same as Ar, the BPASS lines predict less yields than FS for all metallicities with a highly similar general pattern.

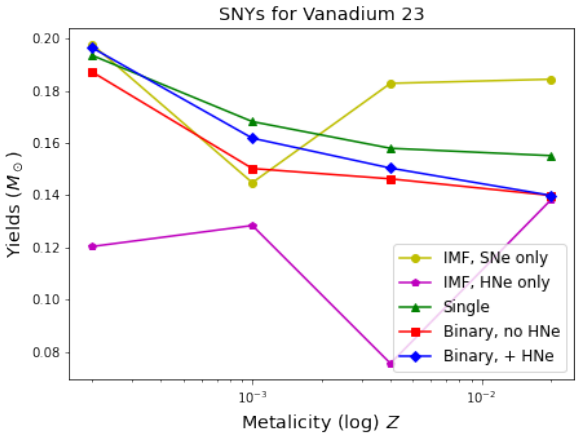


FIG. 29: V, Type S2, shows a weak K pattern. The BPASS lines do not make good approximations to the FS line, the general patterns do not match.

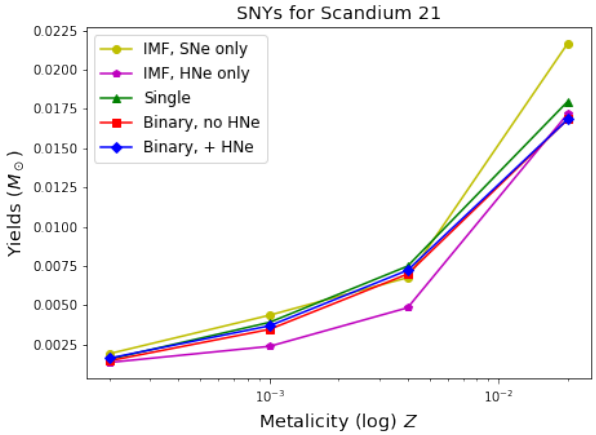


FIG. 27: Sc, Type E1, shows an unclear K pattern. The BPASS lines make good approximations to the FS line.

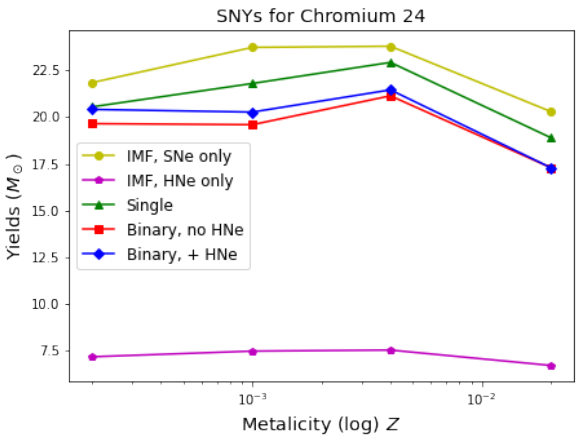


FIG. 30: Cr, Type P, shows a clear strong K pattern. The BPASS lines predict less yields than FS for all metallicities with a highly similar general pattern.

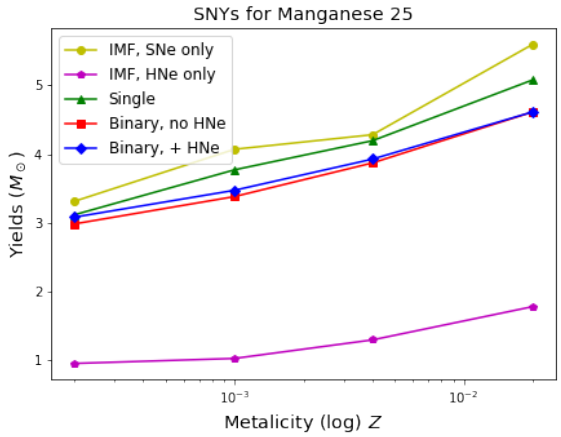


FIG. 31: Mn, Type S1, shows a strong K pattern. The BPASS lines predict slightly less yields than FS for all metallicities with a highly similar general pattern.

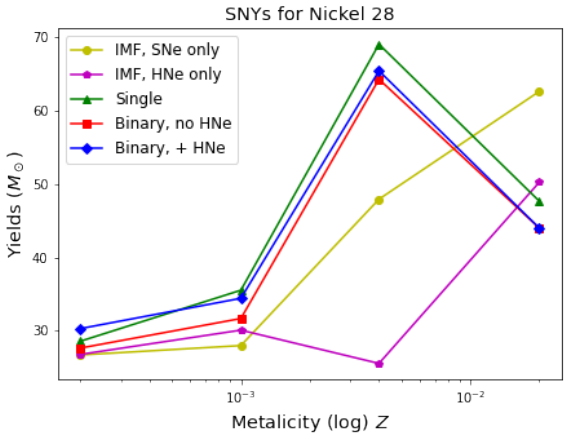


FIG. 34: Ni, Type Λ with a clear peak at $Z = 0.004$, shows a weak K pattern. The BPASS lines do not make good approximations to the FS line, the general patterns do not match.

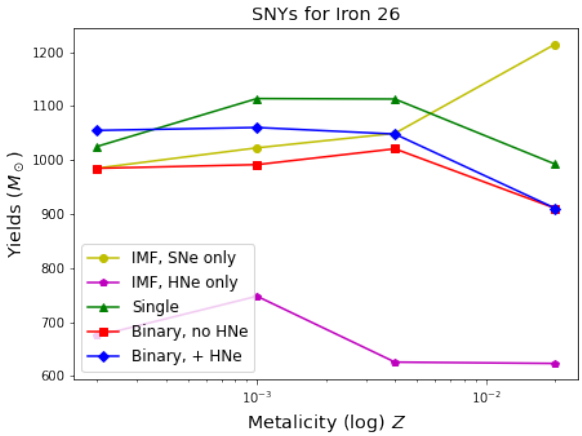


FIG. 32: Fe, Type P, shows a clear weak K pattern. The BPASS lines make not so good approximations to the FS line, the detailed patterns do not match.

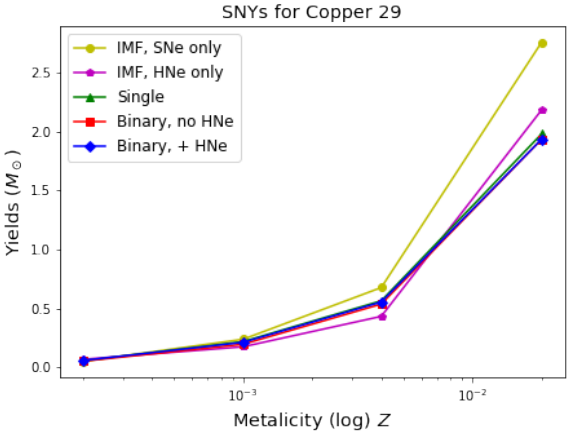


FIG. 35: Cu, Type E1, shows no clear K pattern. The BPASS lines make good approximations to the FS line, with clear lower predictions at $Z = 0.020$.

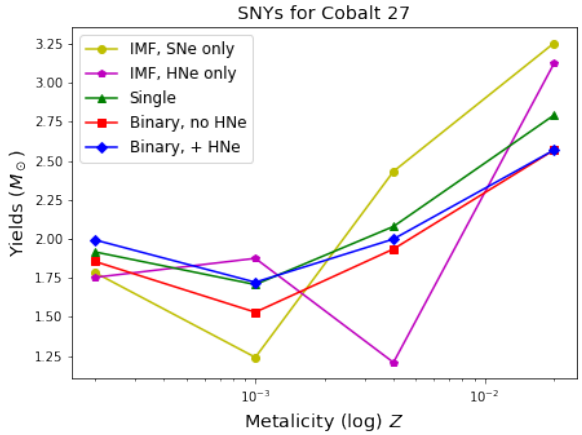


FIG. 33: Co, Type V with a small valley at $Z = 0.001$, shows a weak K pattern. The BPASS predictions agree with lower yields for lower metallicities and higher yields for higher meatallicities than the FS prediction.

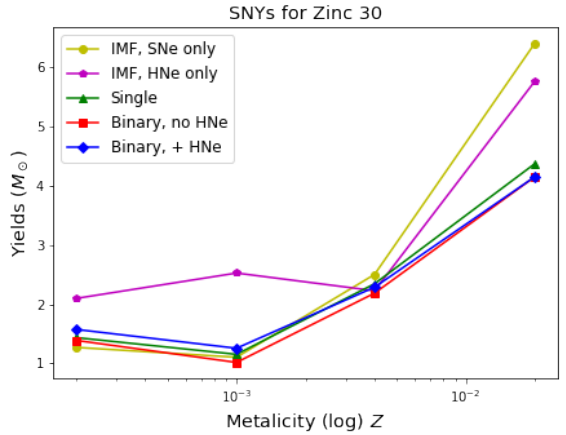


FIG. 36: Zn, Type V with a relative small valley at $Z = 0.001$, shows a weak K pattern. The BPASS lines make acceptable good approximations to the FS line, with 2/3 lower predictions at $Z = 0.020$.

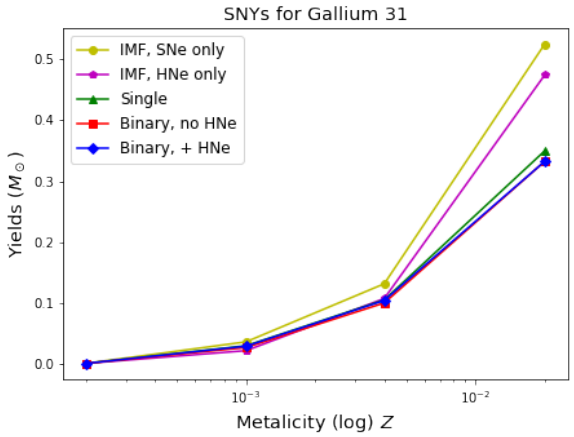


FIG. 37: Ga, Type E1, shows no clear K pattern. Gallium has a highly similar pattern as Cu.

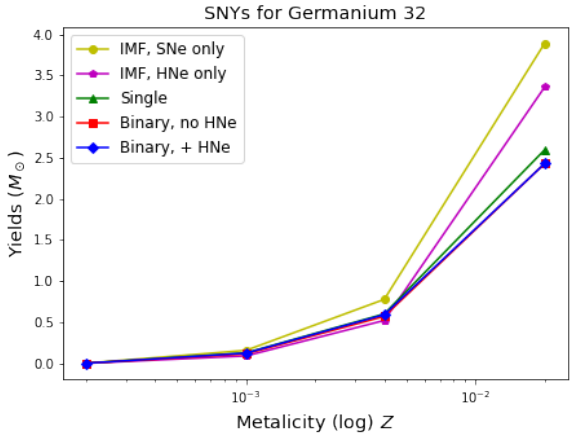


FIG. 38: Ge, Type E1, shows no clear K pattern. Germanium has the same pattern as Ga.

### C. All Plots for Isotopes

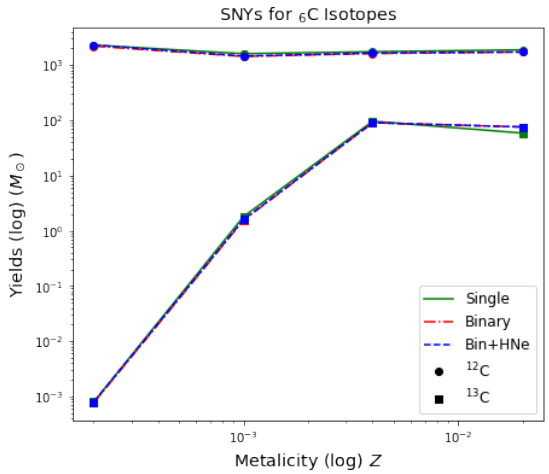


FIG. 39: $^{12}$C is Type S2 and $^{13}$C is Type R1. Binary predicts more $^{13}$C yields at $Z = 0.020$.

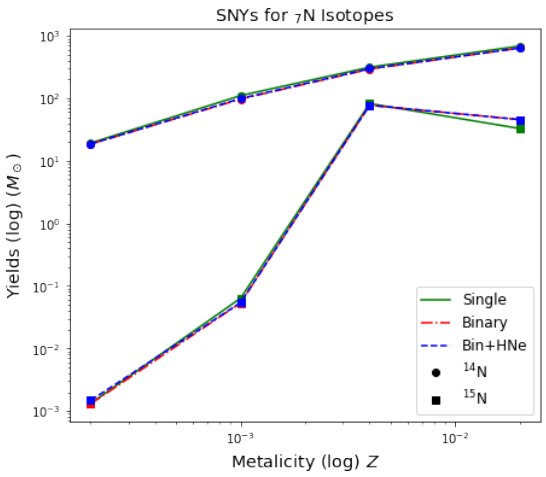


FIG. 40: $^{14}$N is Type M1 and $^{15}$N is Type R1. But $^{15}$N yields reach a small peak at $Z = 0.004$. Binary predicts more $^{15}$N yields at $Z = 0.020$.

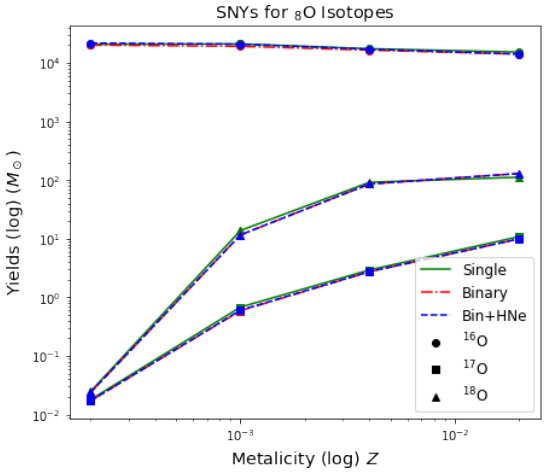


FIG. 41: $^{16}$O is Type S2, both $^{17}$O and $^{18}$O are Type R1. The $^{18}$O yields are higher than the $^{17}$O yields for all metallicties.

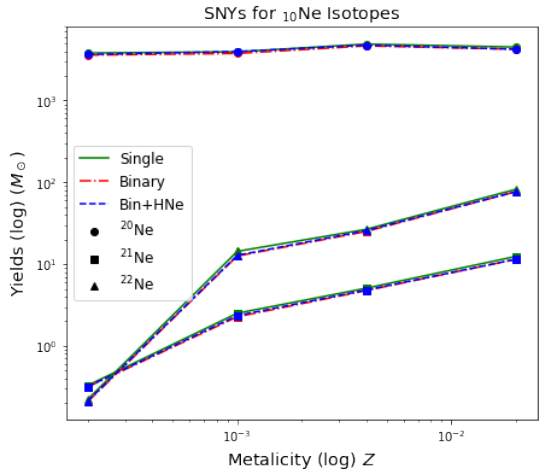


FIG. 42: $^{20}$Ne is Type S1, both $^{21}$Ne and $^{22}$Ne are Type R1. The $^{22}$Ne yields are higher than the $^{21}$Ne yields except $Z = 0.00001$.

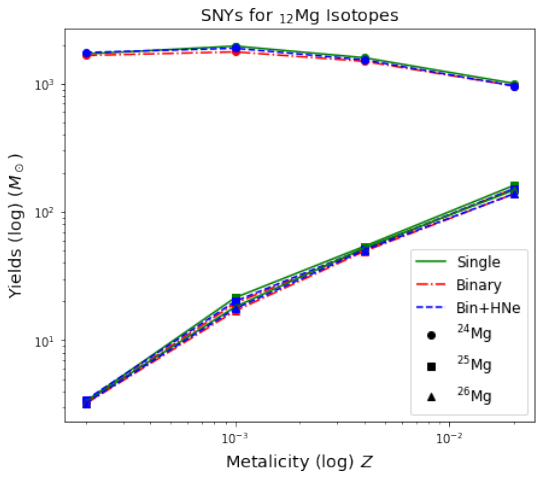


FIG. 43: $^{24}$Mg is Type S2, both $^{25}$Mg and $^{26}$Mg are Type M1 with the same magnitude.

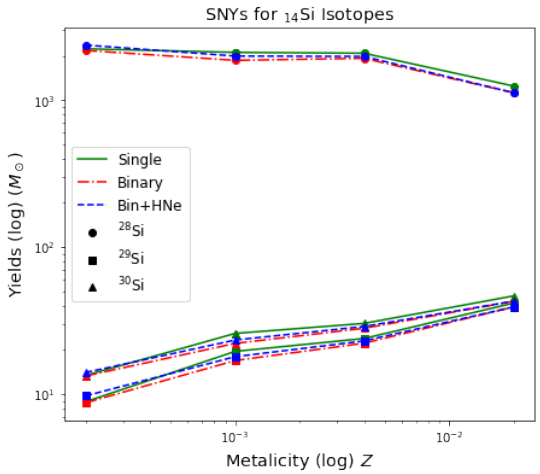


FIG. 44: $^{28}$Si is Type S2, both $^{29}$Si and $^{30}$Si are Type S1. The $^{30}$Si yields are higher than the $^{29}$Si yields for all metallicties. All three isotopes of silicon have weak K patterns.

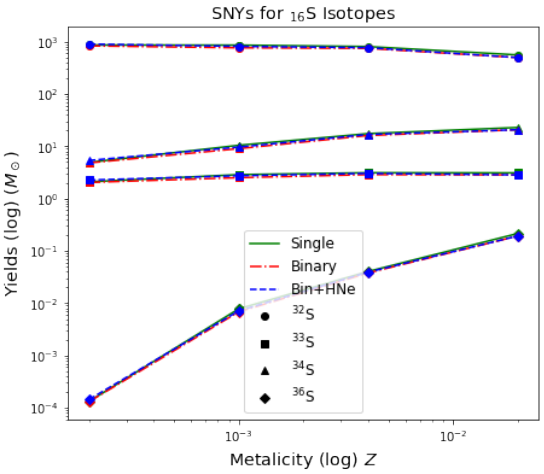


FIG. 45: $^{32}$S is Type S2, $^{33}$S is Type P, $^{34}$S is Type S1 and $^{36}$S is Type R1. Their yields show $^{32}$S $\gg$ $^{34}$S $>$ $^{33}$S $\gg$ $^{36}$S for all metallicties.

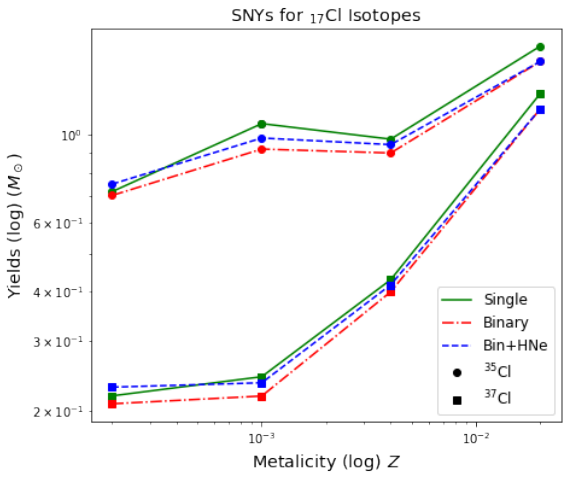


FIG. 46: Both $^{35}$Cl and $^{37}$Cl are Type M1 and show clear weak K patterns.

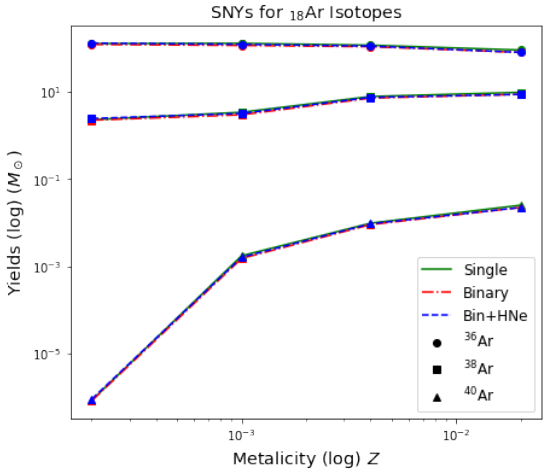


FIG. 47: $^{36}$Ar is Type S2, $^{38}$Ar is Type S1 and $^{40}$Ar is Type R1. For all metallicties, $^{36}$Ar $>$ $^{38}$Ar $\gg$ $^{40}$Ar.

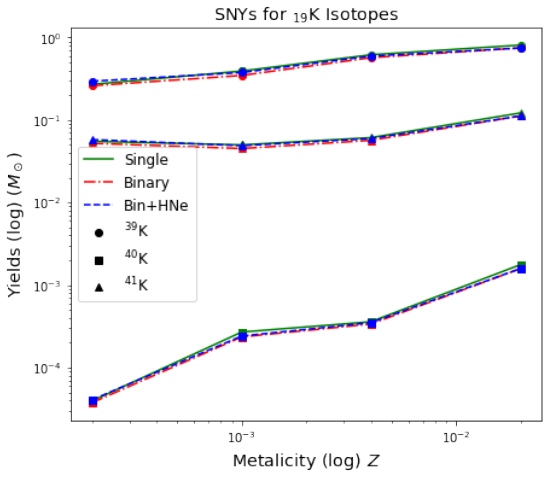


FIG. 48: Both $^{39}$K and $^{41}$K are Type S1 and $^{40}$K is Type M1. For all metallicties, $^{39}$K $>$ $^{41}$K $\gg$ $^{40}$K.

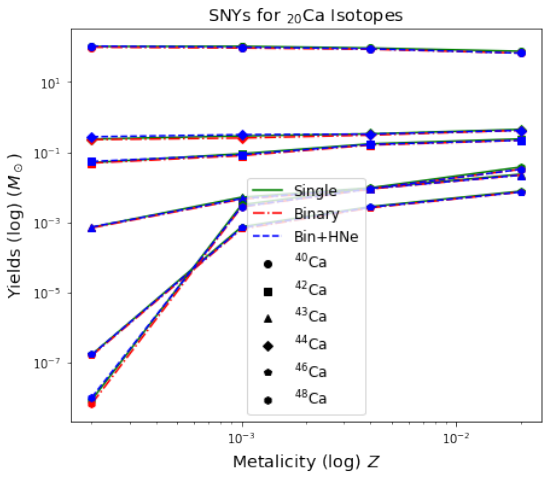


FIG. 49: $^{40}$Ca is Type S2, both $^{42}$Ca and $^{43}$Ca are Type S1, $^{44}$Ca is Type P and both $^{46}$Ca and $^{48}$Ca are Type R1.

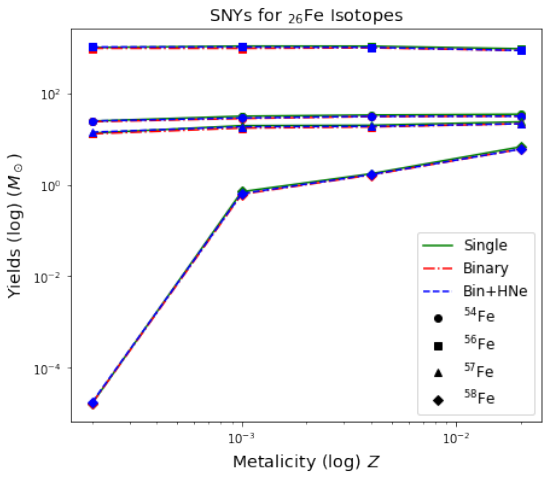


FIG. 52: All $^{54}$Fe, $^{56}$Fe and $^{57}$Fe are Type P, while $^{58}$Fe is Type R1. Notice that the dominant iron isotope is $^{56}$Fe.

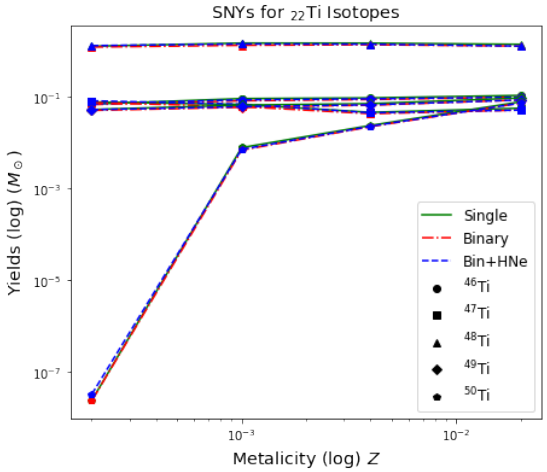


FIG. 50: All $^{46}$Ti, $^{47}$Ti, $^{48}$Ti and $^{49}$Ti are Type P, while $^{50}$Ti is Type R1. Notice that the dominant titanium isotope is $^{48}$Ti.

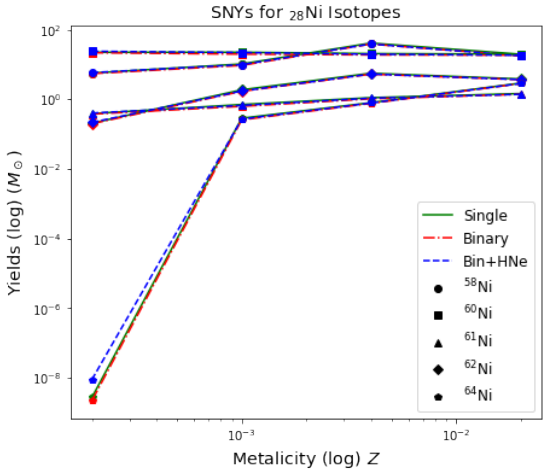


FIG. 53: Both $^{58}$Ni and $^{62}$Ni are Type M1 and reach a peak at $Z = 0.004$, $^{60}$Ni is Type S2, $^{61}$Ni is Type S1 and $^{64}$Ni is Type R1. Notice that the dominant nickle isotopes are $^{58}$Ni and $^{60}$Ni.

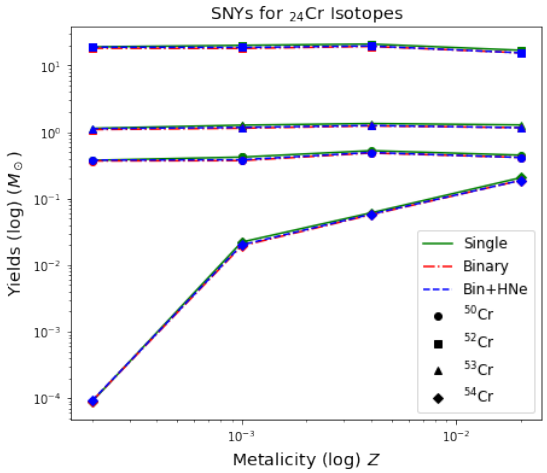


FIG. 51: All $^{50}$Cr, $^{52}$Cr and $^{53}$Cr are Type P, while $^{54}$Cr is Type R1. Notice that the dominant chromium isotope is $^{52}$Cr.

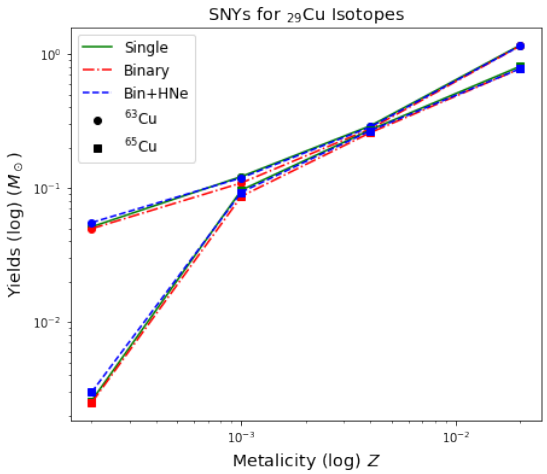


FIG. 54: $^{63}$Cu is Type M1 and $^{65}$Cu is Type R1. $^{63}$Cu is the dominant copper isotope only at $Z = 0.00001$.

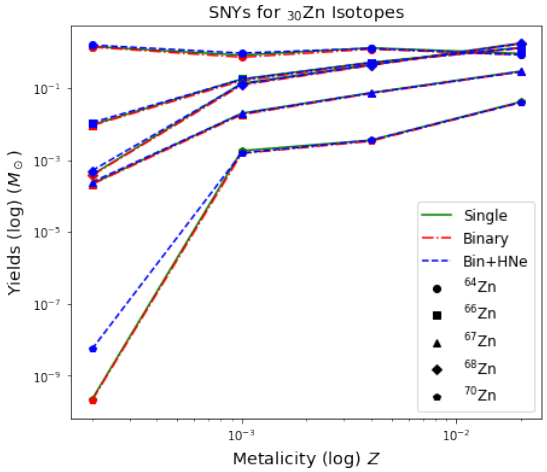


FIG. 55: $^{64}$Zn is Type S2, all $^{66}$Zn, $^{67}$Zn and $^{68}$Zn are Type M1 and $^{70}$Zn is Type R1. $^{64}$Zn is the dominant zinc isotope only at $Z = 0.00001$.

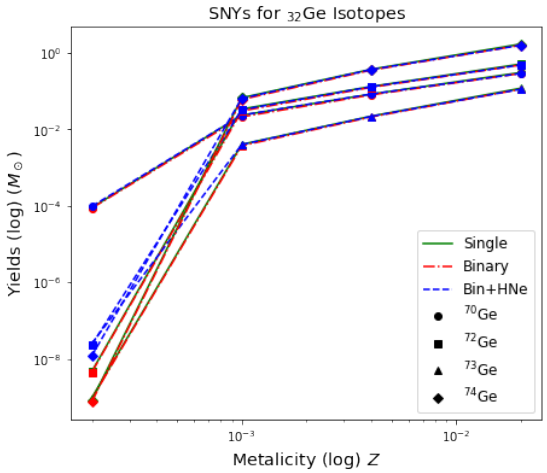


FIG. 56: $^{70}$Ge is Type M1, all $^{72}$Ge, $^{73}$Ge and $^{74}$Ge are Type R1. $^{70}$Ge is the dominant germanium isotope only at $Z = 0.00001$.

**APPENDIX END**